Chapter 3

Fabrication and Characterization of Silk Fibroin Based Nanofibrous Scaffolds Supplemented with Gelatin for Corneal Tissue Engineering

3.1 Introduction

Although gelatin films could provide better cellular biocompatibility and proliferation, it lacks adequate porosity as well as mechanical stability and exhibit brittleness. Silk fibroin (SF) is a naturally occurring, biocompatible, highly stable and mechanically robust polymeric biomaterial that has shown wide applications in tissue engineering and regenerative medicines. SF is generally isolated from cocoons of silkworm (e.g. *Bombyx mori*) and is well known for non-toxicity, tuneable mechanical property, low immunogenicity and high optical transparency across the visible range; however, it lacks suitable porosity and an adequate amount of tripeptide arginine-glycine-aspartic acid (RGD) motifs that help facilitating cellular adhesion. Therefore, cellular growth and proliferation were observed significantly lower when cells were cultured on SF scaffolds alone (Hazra et al. 2016). Moreover, silk film after physical crosslinking possesses low water retention capacity and degradation. Electrospinning of silk fibroin could improve the porosity and water retention capacity, however at the cost of transparency (Varshney et al. 2020; Mitropoulos et al. 2015).

Electrospinning of silk requires usage of harsh conditions such as formic acid, concentrated organic and inorganic salts, ionic liquids or strong acids that lead to dry, mechanically retarded, brittle and opaque nanofibers prohibiting them for corneal tissue engineering applications (Gandhi et al. 2009; Cho et al. 2014; Freddi et al. 1995). Therefore, blending or reinforcing silk nanofibers with other polymers to form composites is envisioned to improve the overall desired properties and this practice has gained considerable interest in last few decades (Cho et al. 2014; Taddei et al. 2013; Mohammadzadehmoghadam and Dong 2019; Farasatkia et al. 2021). Several research efforts have been made and reported in the literature on silk/gelatin blends and their advantages in terms of improved mechanical properties, degradability and

porosity. In particular, Yin et al. fabricated SF/gelatin based nanofibrous scaffolds and revealed enhanced mechanical strength because of gelatin blending (Yin-Guibo et al. 2009). In another work, Mohammadzadehmoghadam et al. developed SF/gelatin blend nanofibers in various ratios of gelatin and silk fibroin and reported a significant increase in the tensile strength (i.e., young's modulus) of the scaffold on addition of gelatin (Mohammadzadehmoghadam and Dong 2019). Moreover, Shan et al. proclaimed enhanced flexibility of the SF/gelatin based nanofibrous scaffolds (Shan et al. 2015). However, to the best of our knowledge, there are no reports on improved transparency of silk/gelatin blend based nanofibrous scaffolds. Furthermore, Ifuku et al. reported that the nanofibrous scaffolds with cavities or porosity could influence the transparency of scaffolds (Ifuku et al. 2013; Nogi et al. 2009). In addition, electrospun nanofiber reinforced polymer composite reduces light scattering and improves the transparency. Nanocomposite film provides flatter and smoother surface resulting in higher transparency and is also expected to exhibit better surface for cellular proliferation (Ifuku et al. 2013; Nogi et al. 2009). Therefore, we adopted a novel polymer composite strategy, wherein silk-gelatin composite scaffold was fabricated to improve the desired features of the cornea tissue. In particular, transparent gelatin composite film containing silk fibroin nanofibers was prepared wherein the silk fibroin nanostructure was anticipated to provide improved mechanical strength and gelatin was presumed to improve limitations of silk nanofibers i.e., ameliorated cellular proliferation and transparency of the scaffold. Furthermore, the fabricated composite scaffold was compared with the existing silk and gelatin based scaffolds such as silk fibroin nanofibers (in aqueous solvent as well as in formic acid) and silk-gelatin blend nanofibers.

In this study, we have proposed a novel, inexpensive gelatin film containing silk nanofibers composite scaffolds (gelatin-permeated SF) for corneal tissue engineering that exhibits good mechanical strength, adequate liquid retention capacity, tunable degradability and excellent transparency comparable to that of native human cornea (Lerman 1984; Beems and Van Best 1990; Hashimoto et al. 2010; Tonsomboon and Oyen 2013) (Table 3.1).

Table 3.1 List of a few-reported scaffolds promising for corneal tissue engineering and their relative properties against our fabricated product.

Reported Scaffolds promising for corneal tissue alternatives	**Essential properties required for corneal scaffolds**			
	Transparency	**Mechanical Stability**	**Porosity**	**Cellular biocompatibility**
Collagen-based split thickness cornea substitute (Acun and Hasirci 2014)	~80%	NA	~70%	Suitable for human corneal keratocytes (HK) and retinal pigment epithelium (RPE) cell attachment and proliferation
Oriented nanofibrous silk scaffold (Biazar et al. 2015)	NA	NA	NA	All limbal stem cells maintained their characteristic features.
Electrospun gelatin fiber-alginate gel composite nanofibrous scaffolds (Tonsomboon and Oyen 2013)	30%-60% (Gelatin fiber-alginate hydrogel scaffold)	0.45– 0.5 MPa (Gelatin fiber-alginate hydrogel scaffold)	NA	NA
Non-mulberry silk fibroin film (Hazra et al. 2016)	~94%	Intraocular pressure did not vary significantly after implantation	NA	Support corneal cell and biocompatible in rabbit eyes

Cellulose nanofiber reinforced silk fibroin composite scaffold (Cho et al. 2014)	~75%	70.9 ± 6.6 MPa	NA	NA
Silk fibroin/gelatin blend film (Taddei et al. 2013)	NA	108.0 ± 20.1 MPa	NA	C2C12 cardiomyocytes showed that crosslinked silk fibroin/gelatin (SF/G) blends containing a SF ≥ 60 wt % supported cell adhesion and proliferation after 72 h culture time (~ 68% with respect to control)
Electrospun silk fibroin/Gelatin blend Scaffold (Mohammadzadehmoghadam and Dong 2019)	NA	~16 MPa	NA	Silk fibroin/gelatin blend ratio 70/30 (% w/w) demonstrated the lowest 3T3 fibroblast cell responses for proliferation rates.
Silk nanofibrils (SNF)/gelatin methacryloyl (GelMA) [S/G] composite scaffold (Farasatkia et al. 2021)	SNF/GelMA ratio of 30/70 (% v/v) shows high transparency with a light transmittance of more than 85%	437.5 ± 29 kPa	Pore size 28 ± 8 μm (for GelMA) to 22 ± 7 μm (for 30S/70G (%v/v)	SNF/GelMA nanohybrid exhibited as an attractive candidate for corneal cell regeneration (97 ± 2% of the area of SF/G scaffold covered with cells after 5 days of culture)
Electrospun nanocomposite silk nanofibers supplemented with gelatin scaffold (Our fabricated product)	77.75 ± 2.3 %	12.56 ± 0.69 MPa	47.30 ± 0.90 %	Significant rabbit corneal fibroblast (SIRC) cell and mouse fibroblast

				(L929-RFP) cell growth and proliferation [69% (SIRC) and 71% (L929-RFP) by 6 days in culture]
Native human cornea	70%- 95% depending upon the age group. (Beems and Van Best 1990; Lerman 1984)	0.579 - 4.9 MPa (Tonsomboon and Oyen 2013)		

This chapter describes an attempt towards the development of composite scaffolds for corneal stromal equivalent by utilizing both silk and gelatin biopolymers. Silk fibroin mats were fabricated in both i.e., SF (in aqueous; treated (T) and non-treated (NT)) and SF (in formic acid; treated (T) and non-treated (NT)); and gelatin-permeated SF (in formic acid; treated (T) and non-treated (NT)) scaffolds. The fabricated composite scaffolds were studied and evaluated for their suitability as corneal stromal analogs with respect to mechanical stability, liquid retention capacity, transparency and cellular biocompatibility.

3.2 Materials and method

3.2.1 Materials

Bombyx mori cocoons were procured from Research Extension (Silk Board), Bhadrasi, Varanasi, Ministry of Textiles, Government of India. Gelatin type A (Bloom 300) was procured from Sigma Aldrich, India. Dialysis membrane [12,000 Molecular Weight Cut Off (MWCO)], polyethylene glycol (PEG, molecular weight- 20,000), lithium bromide (LiBr), phosphate buffer saline (PBS), 3–(4,5-dimethyl-2-thiazolyl)-2, 5-diphenyl-2 tetrazolium

bromide (MTT), Dulbecco's modified Eagle's medium (DMEM) high glucose, fetal bovine serum (FBS), antibiotics penicillin and streptomycin solution (100X), were purchased from HiMedia, India. Absolute ethanol 99.9% of high analytical grade and distilled water were used in all the experiments. Glacial acetic acid (GAA), ethyl acetate, sodium carbonate (Na_2CO_3) were purchased for SRL, India.

3.2.2 Methods

3.2.2.1 Preparation of Silk Fibroin Solution.

The silk fibroin (SF) solution was isolated from silk cocoons as described earlier in chapter 3 and as per the standard protocol (Chouhan et al. 2017; Rockwood et al. 2011). The resulting solution was 7-8% (w/v) which was further concentrated to 14-16% using 10% (w/v) PEG (MW. 20k) continuously stirring at 4°C for 10 h. The concentrated silk fibroin solution was stored at 4°C until usage (The silk solution was utilized within 2 weeks of extraction).

3.2.2.2 Fabrication of electrospun nanofibrous mats

Electrospinning the polymer must form the Taylor cone that depends on various parameters as shown in the Taylor cone equation below, to enable the formation of fiber jets.

$$\left(\frac{V_C}{H}\right)^2 = \frac{4}{L^2}\left(\ln\frac{2L}{R} - \frac{3}{2}\right)(0.117\pi\gamma R)$$

Where V_c is the critical voltage, H is the distance between capillary tip and the grounded collector. L and R denote length and radius of the needle, respectively. ɣ denotes the surface tension of the solution which acts as one of the crucial factors for Taylor cone generation, provided H, L and R remain constant (Ahearne et al.; Kishimoto et al. 2017a; 2018; Yao et al. 2003). According to the equation, it is necessary to optimize a required level of surface tension of the solution for the given values of V_c, H, L and R to create bead-free nanofibrous sheets.

Silk fibroin solution was air-dried inside a laminar airflow cabinet. Air dried silk films were dissolved in formic acid (98%) followed by continuous stirring for preparation of 10% (w/v) silk solution SF (in formic acid; NT). The solution was stirred at 37°C for 4 hours and left to cool at a room temperature (25°C) prior to electrospinning and utilized fresh. The silk nanofibrous scaffold was fabricated using electrospinning machine (E-spin nanotech, India). Briefly, the solution was filled in a 10 mL syringe and sprayed with a flow rate of 0.40 ± 0.10 mL/h via a 21-gauge needle (Table 3.2).

Table 3.2 Optimized values of electrospinning parameters for the prepared formulations.

Parameters	**Optimized value for silk in aqueous solvent SF (in aqueous)**	**Optimized value of silk in formic acid SF (in formic acid)**
Flow rate	0.4± 0.1 mL/h	0.4± 0.1 mL/h
Applied high voltage	15 ± 2 kV	20 ± 2 kV
Distance between needle and drum collector	15 centimeter	15 centimeter
Needle size	22 gauge with bevel tip	22 gauge with bevel tip
Syringe inner diameter	16 mm	16 mm
Syringe volume	10 mL	10 mL
Total time	36 h	36 h
Collector	Drum collector (rotating)	Drum collector (rotating)

Various parameters such as flow rate, sample concentration, applied voltage and the distance between the needle and collector were selected with multiple values while optimizing for nanofiber formation. Most of the values such as sample concentration, sample solvents, and distance between needle and collected were cited from Cao et al., and Mohammadzadehmoghadam et al. to get a basis of electrospinning of silk in formic acid and in aqueous state (Cao et al. 2009; Mohammadzadehmoghadam and Dong 2019; Cestari et al. 2014). Few parameters such as syringe volume and flow rate were already provided in the user

manual instructions of the instrument (espin nanotech, IIT Kanpur). Rest of the parameters such as applied voltage and thickness of the scaffold were optimized after multiple attempts. The drum collector (at a rotating speed of 1000 rpm) was placed at 15 cm away from the needle. The high voltage applied was around 15 ± 2 kV for 36 h. For electrospinning of aqueous silk SF (in aqueous; NT) the selected fibroin concentration was around 7-8 % (w/v). The applied voltage was slightly higher i.e., 20 kV and rest of the conditions were similar to that used for silk in formic acid SF (in formic acid; NT). The obtained silk SF (in aqueous; NT) mat was further treated overnight with 70% (v/v) ethanol vapor to enhance β sheets inside the electrospun silk mats.

3.2.2.3 Permeation of gelatin solution inside electrospun silk scaffolds

The gelatin powder was dissolved in deionized water to prepare a gelatin solution (10% w/v) and stirred continuously at 40°C for 1 h. The resulting concentrated gelatin (10% w/v) was spin coated at 500 rpm for 7 minutes at an acceleration of ~500 to obtain a thickness around ~300-400 μm on the polystyrene substrate. Furthermore, the electrospun silk mat (in formic acid) was placed on the top of spin coated gelatin gently, which allowed permeation of gelatin in all the unoccupied space in-between the nanofiber space. The gelatin-permeated SF (in formic acid; NT) scaffold was further dried overnight at room temperature and the dried scaffold was further treated with 70% ethanol overnight.

3.2.3 Characterization of the scaffolds

3.2.3.1 Morphological characterization of electrospun nanofibers

The nanofibers arrangement, their pore size distribution and morphological characteristics of the scaffolds were determined using scanning electron microscope (Zeiss EVO 18 SEM Zeiss, Oberkochen, (Germany)) with an accelerating voltage of 20 kV. The prepared samples were

dried and cut into 10 × 10 mm dimension, followed by sputter gold coating to make the exposed surface conductive. The SEM micrographs were captured at 3 different magnifications i.e., at 5k, 10k and 25k, at an accelerating voltages of 15 KeV. The coated scaffolds were then observed under SEM to determine the extent of porosity, gelatin permeation inside the scaffold and surface morphology. Moreover, pore size distribution was analyzed using ImageJ software.

3.2.3.2 Porosity determination

The fiber diameter and the porosity of the nanofibrous scaffolds were manually measured using an ImageJ software (NIH, USA) from at least 5 different images of each type of scaffold (average diameter of 90-100 nanofibers was examined in each image). All the images were converted to binary format followed by base scale setting. Furthermore, images were cropped and set mean threshold for image processing and the final porous area percentage was calculated. For porosity measurement, we performed image analysis using an ImageJ software, which was proposed to deliver the reliability of a 95% confidence level (Michalak et al. 2017). The ranges of the fiber diameter and fiber orientation within the scaffolds were plotted using the Origin software (OriginLab Corporation).

3.2.3.3 ATR-FTIR analysis

Infrared spectra for the scaffolds were recorded on Nicolet iS5 THERMO Electron Scientific Instruments LLC equipped with diamond laminate crystal with iD5 attenuated total reflection (ATR) accessory. 4 cm^{-1} resolutions with 16 scans were taken for all spectra at an infrared range of 500– 4000 cm^{-1}.

3.2.3.4 Liquid retention capacity

The liquid absorption capability of the scaffolds was discerned by soaking the scaffolds in phosphate-buffered saline (PBS), pH 7.4 at a room temperature for 48 h. Scaffolds used for this study were 10 mm × 10 mm × 0.5 mm (l×b×h). The water absorption ratio is defined as the ratio of final weight to the initial weight. The weight of the wet scaffolds was measured immediately by blotting the surrounding water content with the help of a tissue paper. Each sample was assessed in triplicates for their swelling and absorption.

3.2.3.5 In vitro stability and degradation

In vitro stability and biodegradation of the fabricated scaffolds were carried out in a PBS solution (pH 7.4) as well as in a lysozyme solution (10^4 U/mL in distilled water) at a room temperature and at 37°C inside a humidified CO_2 incubator. The scaffolds were kept in the medium for 14 days with a change in the medium on every alternate day. The lysozyme degradation was observed after 14 days of incubation. The scaffolds were weighed at regular time intervals while changing the degrading medium. At the end of the stipulated time period the scaffolds were lyophilized for SEM analysis. The degradation percentage was quantified using the following formula-

$$Degradation\ (\%) = \left(\frac{W_i - W_f}{W_i}\right) \times 100$$

Where W_i and W_f are the initial and final weights of the scaffolds before and after degradation, respectively (Varshney et al. 2019).

3.2.3.6 Transparency determination

Transparency of all the scaffolds was measured quantitatively using a UV-visible spectrophotometer (UV-VIS Spectrophotometer – 2373, Electronics India (EI), India) across

the range of visible wavelengths (400-700 nm). The scaffolds were cut into strips with dimensions of 30 x 9 mm with a thickness range of 0.4 - 0.5 mm. The scaffolds were stored in PBS and loaded in a cuvette for transparency measurement. The cuvette containing the samples were place in a cuvette holder and percentage transmission spectra of the samples were measured with scanning in the range of visible wavelengths (400-700 nm). Cuvette with PBS solution was measured as a reference to set the baseline. 10 mm circles of each scaffolds were punched and placed on green background with number '0' painted on it. The physical appearance of the number written below the scaffold provides a glimpse about the transparency of the corresponding scaffolds.

3.2.3.7 Water contact angle measurement

Contact angles of the fabricated scaffolds (treated and non-treated with ethanol) were measured using the ImageJ technique. We have utilized Fiji (Fiji is just ImageJ) software to evaluate the contact angle. 10 µL deionized water drop was dispensed on the sample surface with a micropipette and the contact angle was measured. The image of the drop on the surface was captured using high resolution digital camera (Canon 1500D). DropSnake ImageJ plugin method was applied to determine the contact angle of the droplet. All measurements were carried out with deionized water and each sample was measured with a minimum of 3 drops.

3.2.3.8 Mechanical testing of the Scaffold

Mechanical stability of the scaffolds plays a key role for its applications in tissue engineering, especially in case of fabricating artificial corneas as they bear high intraocular pressure. Mechanical properties of the electrospun nanofibrous samples were quantified using texture analyzer (CT3 Texture analyzer, Brookfield). The instrument was equipped with 5 kN load cell and the tensile testing was assessed with a cross-head speed of 5 mm/minute until failure.

The tested specimens were rectangular strips measuring 60 ×10 mm, with a thickness around 0.5 ± 0.2 mm. Average sample thickness was calculated by measuring thickness at 5 different positions of the nanofibers mat. At least three independent tests were conducted for each sample to measure the tensile strength.

3.2.4 Cellular viability and compatibility

3.2.4.1 Culturing of cells within scaffolds

The SIRC [Statens Seruminstitut Rabbit Cornea] fibroblasts cells and L929-RFP (red fluorescent protein) cell lines, which are rabbit corneal fibroblast and mouse fibroblast cells, respectively, were used as the cells of choice for this study. The cells were maintained in a complete growth culture medium at 37°C along with the supply of 5% CO_2 and appropriate levels of humidity. The complete growth culture medium comprised of Dulbecco's modified Eagle's medium (DMEM, HiMedia) supplemented with 10% fetal bovine serum (FBS, HiMedia) and 1% penicillin/streptomycin antibiotics (HiMedia). The scaffold circular discs were punched out using a 6 mm biopsy punch and the cells were seeded on top surface of the electrospun nanofibrous scaffolds at a density of 1×10^4 cells per scaffold. The cell seeded scaffolds were left in a 35 mm Petri dish for cell adherence with scaffold in a CO_2 incubator at 37°C. After half an hour, the culture plates were filled with 2 mL of complete growth medium. The scaffolds were regularly shifted to fresh plates to avoid interference during observation of the cells inside the scaffolds from those adhered on the tissue culture plates. For imaging, the cells laden scaffolds were shifted to new Petri plates to avoid the interference of cells that were migrated to the bottom surface of the Petri dish during the incubation period.

3.2.4.2 Nuclear staining

For the visualization of SIRC cells within the scaffold, cellular nuclei were stained with 4,6-diamidino-2-phenylindole (DAPI) (1 µg/mL). The DAPI stain imparts blue colour when on binding at the A-T rich region in the DNA. For DAPI staining, culture media of the plate containing scaffolds were discarded and the scaffolds were washed thrice with PBS followed by fixation of the cells using 4% paraformaldehyde for 30 minutes at a room temperature. Furthermore, the cells were washed again using PBS and incubated with 0.1% (v/v) triton X-100 for 10 minutes. 1% bovine serum albumin (BSA) solution prepared in PBS was added to block the non-specific binding of the stain (for 30 minutes) followed by washing with PBS to remove excess unbound BSA. The scaffolds were incubated with DAPI stain for 30 minutes in dark environment. Finally, the scaffolds were again washed three times using PBS to remove unbound DAPI stains followed by addition of 80% glycerol to prevent the scaffold from desiccation. Finally, the scaffolds were observed under the fluorescent microscope.

3.2.4.3 MTT assay

Cell proliferation and toxicity were determined by a 3-[4, 5-dimethyl-thiazol-2-yl]-2,5-diphenyltetrazolium bromide [MTT] (HiMedia, India) reduction assay using a SIRC [Statens Seruminstitut Rabbit Cornea] cell line (procured from NCCS, Pune). Briefly, this assay is based on the principle that metabolically active cells reduce yellow color tetrazolium MTT into intracellular purple formazan through dehydrogenase enzyme activity (as described in chapter 3). This purple colour formazan was quantified via a standard microplate absorbance reader after solubilization with dimethyl sulfoxide (DMSO). The rate of cell proliferation is reciprocal to the rate of tetrazolium reduction. The MTT assay was performed on both SF (in aqueous; T) and gelatin-permeated SF (in formic acid; T) scaffolds placed at the bottom of a 96-well

plate following the standard procedure. Cells were maintained in DMEM supplemented with serum and antibiotics at 37°C in a 5% CO_2 humidified incubator. 6 mm scaffold discs were punched out and sterilized by exposing them to ultra-violet radiation for 1 h inside the biosafety cabinet. Cells cultured in the well were regarded as positive control and the scaffold in the well without cells (rest all the conditions were same as to the test samples) were marked as negative control. SIRC cells were seeded on each scaffold at a density of 1×10^4 cells/mL and maintained in a CO_2 incubator for 2, 4 and 6 days. After incubation, the culture medium was removed from each well and a total of 100 µL solution of medium and MTT (5 mg/mL in PBS) solution in the ratio of 10:1 were added to each well and incubated. After 4 h of incubation with MTT, the medium containing MTT was removed. The formazan crystals formed inside the wells were solubilized using a 100 µL dimethyl sulfoxide (DMSO, HiMedia) solution for 15 min. The optical absorbance was measured at 570 nm on a multiplate reader (Synergy H1 hybrid, Biotek, USA). Each experiment was carried out in triplicates for testing cytotoxicity and biocompatibility of the scaffolds.

3.2.4.4 Statistical Analysis

All the experiments were performed in triplicates, unless otherwise stated and the results were expressed as mean ± standard deviation (SD). For the statistical analysis, one-way ANOVA was performed for all the samples wherever it was required. To assess the difference between groups, one-way ANOVA was followed by Tukey's multiple comparison test between the groups and considered significant when $p < 0.05$ *, $p < 0.01$**, $p < 0.001$***. Background noise was removed from fluorescent images through ImageJ software. Gaussian blur function was applied individually to convolve the image followed by subtraction from respective raw fluorescent images to elude the background noise.

3.3 Results

3.3.1 Characterization of the scaffolds

3.3.1.1 Morphological characterization of electrospun nanofibers

After 24 hours of electrospinning of the silk solution prepared in formic acid solvent, 0.4 - 0.5 mm thick electrospun silk nanofibrous mat SF (in formic acid; NT) was obtained on aluminum foil wrapped around cylindrical collector mandrel with nanofiber diameters majorly falling around 100-140 nm. Uniform and bead free, randomly oriented nanofibrous silk scaffolds were obtained and confirmed using obtained SEM images (Figure 3.1). The figure 3.1(a) represents the digital images and their respective SEM images of all three types of fabricated scaffolds. The silk fibroin in aqueous solvent SF (in aqueous; NT) resulted in microbeads based electrospun sheet with a negligible amount of nanofibers connecting the beads. The formation of microbeads of SF (in aqueous; NT) could be attributed to the process of electro-spraying instead of electrospinning; as the electrospinning of any polymer relies on surface tension, viscosity, critical voltage and certain other factors. It has already been reported that during electrospinning the polymer must form the Taylor cone (as discussed in method section). Figure 3.1(b) represents the digital images and their respective SEM images of all three types of fabricated scaffolds after ethanol vapor treatment. Morphological evaluation of gelatin-permeated SF (in formic acid; NT) from the SEM images obtained at five different positions of the random cross section represents negligible or no sign of any bubble entrapment in between the nanofibrous structures. These results suggested that gelatin got permeated continuously throughout the silk nanofibrous mats without leaving any air space (Figure 3.2).

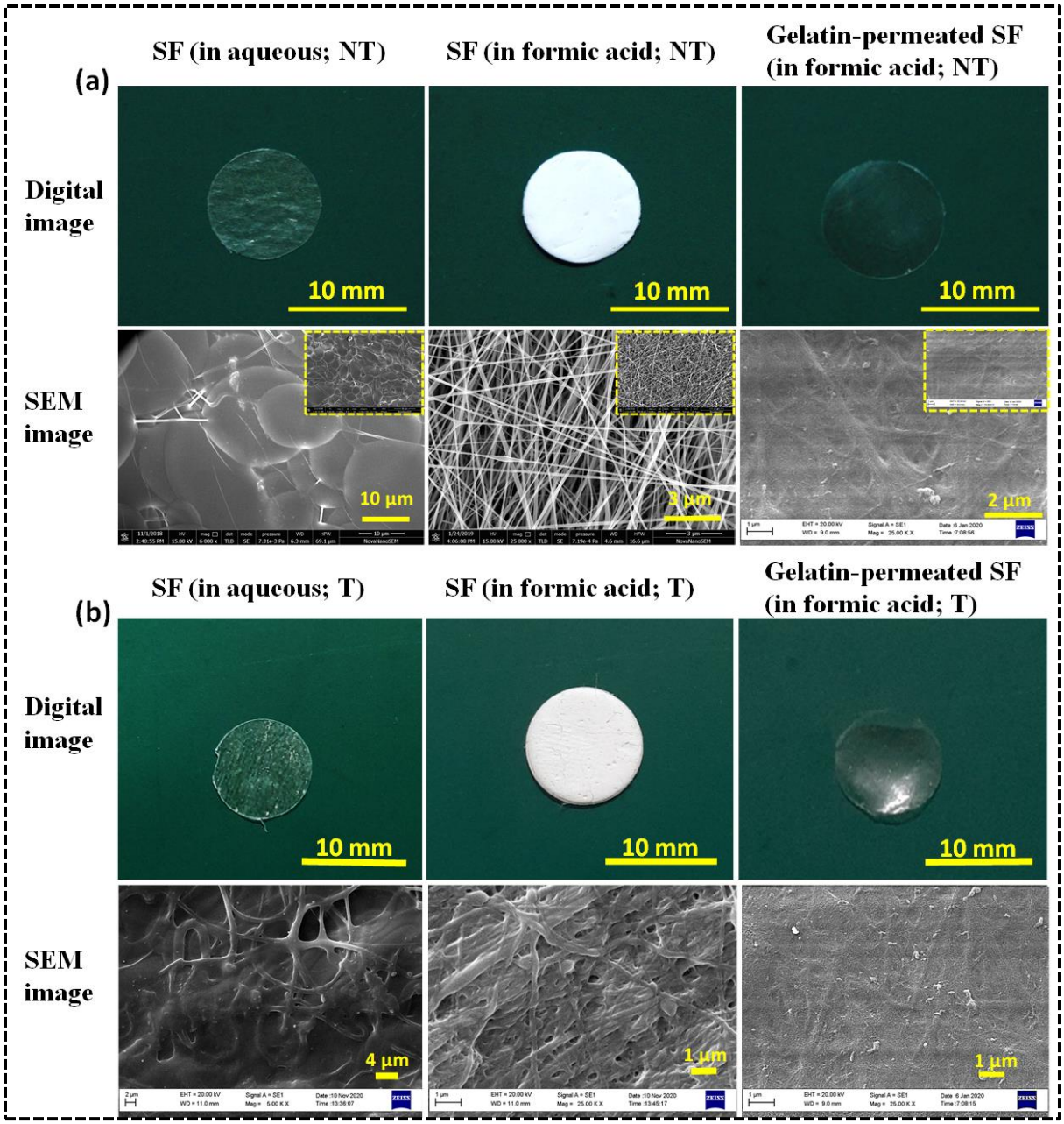

Figure 3.1 Morphological analysis through SEM photomicrographs of SF (in aqueous), SF (in formic acid) and gelatin-permeated SF (in formic acid); scaffolds along with their respective digital images (a) before ethanol vapor treatment i.e., SF (in aqueous; NT), SF (in formic acid; NT), gelatin-permeated SF (in formic acid; NT) and (b) after ethanol vapor treatment i.e., SF (in aqueous; T), SF (in formic acid; T), gelatin-permeated SF (in formic acid; T).

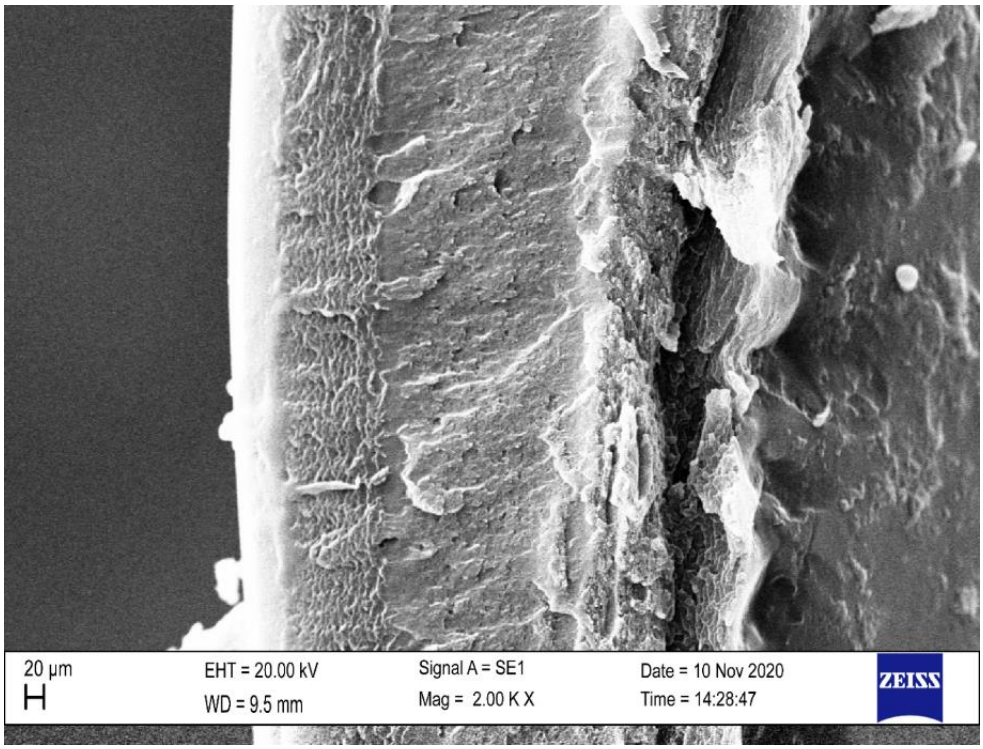

Figure 3.2 Representative image shows continuous gelatin permeation throughout the internal space of the silk nanofibrous scaffold gelatin-permeated SF (in formic acid) without leaving any air space along with negligible or no sign of any bubble entrapment within the nanofibrous structure. Scaffolds were cut across the longitudinal plane to observe the extent of gelatin permeation through the SEM.

3.3.1.2 Porosity determination

The SEM micrograph was utilized for the calculation of fiber diameter, fiber orientation and the porosity within the nanofibrous scaffolds by ImageJ (open, free software for image processing). The 'mean' factor was adopted to determine the threshold value. The porosity of the nanofibrous structure was calculated from the unoccupied spaces in between the nanofibrous structures. Obtained results of SF (in formic acid; NT) scaffolds showed porosity values around 47.30 ± 0.90%. The result depicted fiber diameters ranging from 40 nm to 320 nm, out of which the majority of the fiber diameter lied in the range of 100 nm – 140 nm (Figure 3.3).

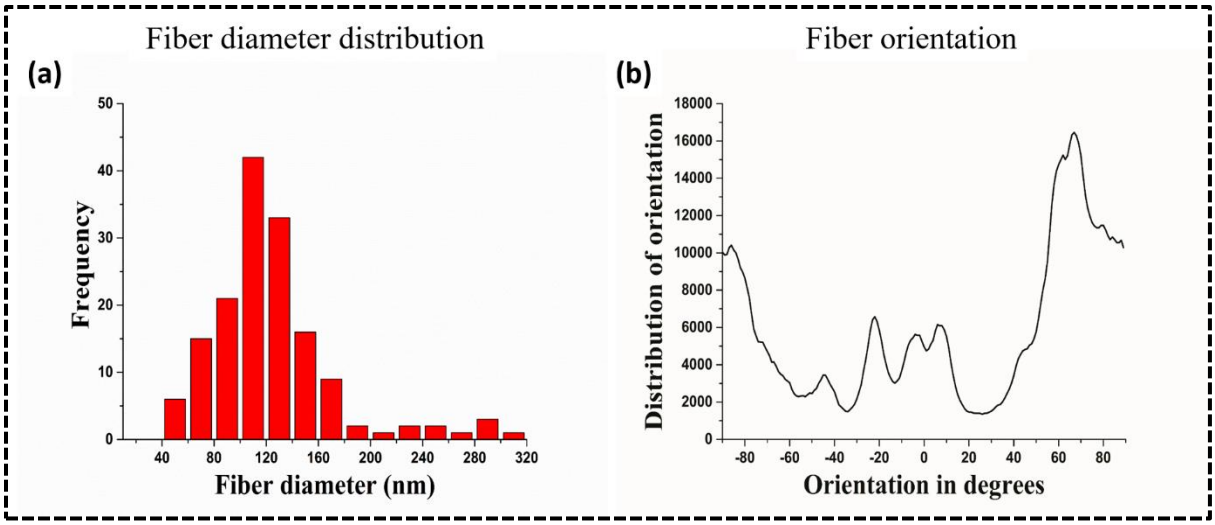

Figure 3.3 Diameter distribution of nanofibers of electrospun SF (in formic acid; NT) scaffolds along with its nanofiber orientation graph.

The nanofibers were majorly oriented in an aligned manner with a few randomly oriented nanofibrous arrangement. It was difficult to determine the porosity of SF (in aqueous; NT), SF (in aqueous; T), gelatin-permeated SF (in formic acid; NT) and gelatin-permeated SF (in formic acid; T) using ImageJ, because of unavailability of the free porous spaces. A significant reduction in the level of porosity was observed in SF (in formic acid; T) nanofibrous scaffolds treated with ethanol (Figure 3.1) (Yang et al. 2012).

3.3.1.3 ATR-FTIR spectroscopic analysis

ATR-FTIR spectroscopy was performed to quantify the presence of respective functional groups within the nanofibrous scaffolds and to study the effect of ethanol treatment on the respective scaffolds. FTIR spectrum of SF (in aqueous; NT), SF (in formic acid; NT), gelatin-permeated SF (in formic acid; NT), SF (in aqueous; T), SF (in formic acid; T) and gelatin-permeated SF (in formic acid; T) has been shown in figure 3.4.

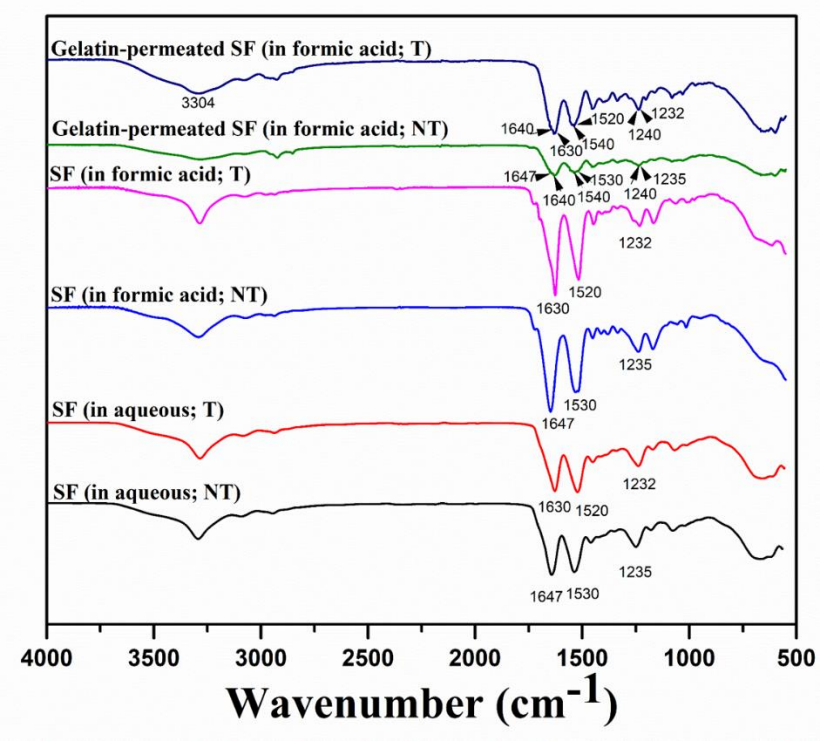

Figure 3.4 ATR-FTIR spectra of SF (in aqueous; NT), SF (in formic acid; NT), gelatin-permeated SF (in formic acid; NT), SF (in aqueous; T), SF (in formic acid; T) and gelatin-permeated SF (in formic acid; T). (where NT= non-treated, T= ethanol treated).

The major peaks of SF (in aqueous; NT) and SF (in formic acid; NT) scaffolds were detected at 1647, 1530 and 1235 cm^{-1}. These absorption peaks correspond to peptide backbone of amide I (C=O stretching), amide II (N-H Bending) and amide III (C-N stretching), respectively. These amide I, amide II and amide III could be attributed to random coil and silk I structure. Overnight ethanol vapor treatment led to shift in the absorption peaks to a slightly lower wavenumber i.e., at 1630 cm^{-1}, 1520 cm^{-1} and 1232 cm^{-1} for amide I, amide II and amide III, respectively; attributing to β sheet formation and indicating SF (in aqueous; T) and SF (in formic acid; T) mainly exhibited silk II structure. Characteristic absorption peaks of gelatin could be identified at 1640 cm^{-1} (C=O stretching) for amide I, 1539 cm^{-1} (N-H bending vibrations and stretching vibrations of C-N) for amide-II, 1240 cm^{-1} (N-H in phase bending and C-N stretching) for amide-III and 3304 cm^{-1} represents for amide A (N-H stretching vibration). Silk nanofibrous scaffold permeated with gelatin-permeated SF (in formic acid;

NT) represents all the characteristic absorption peaks of both silk and gelatin. Gelatin-permeated SF (in formic acid; T) follows the similar trend of gelatin-permeated SF (in formic acid; NT) with a little shift in silk absorption peaks at 1630 cm^{-1}, 1520 cm^{-1} and 1232 cm^{-1} for amide I, amide II and amide III, respectively, with certain adjustment in the respective intensities of the peaks (Amiraliyan, Nouri, and Haghighat Kish 2010; Okhawilai et al. 2010; Shen et al. 2015; Yusoff et al. 2019).

3.3.1.4 Liquid retention capacity

The results for fluid retention ability of the ethanol treated scaffolds are shown in figure 3.5. The fluid retention capacity of the fabricated scaffold was examined in terms of percentage weight gain when immersed in PBS over a period of 48 h. SF (in aqueous; T) depicted least liquid retention capacity due to its negligible pore size compared to SF (in formic acid; NT) and SF (in formic acid; T) where available pore size was found significantly higher. SF (in aqueous; NT), SF (in formic acid; NT) and gelatin-permeated SF (in formic acid; NT) exhibited total weight gain higher than their respective ethanol treated forms i.e., ~ 415%, ~ 515% and 740%, respectively, but started losing weight after 6 h of incubation due to degradation. SF (in aqueous; T) scaffolds showed ~300% gain while SF (in formic acid; T) depicted ~450% gain from their initial dry weight, whereas gelatin permeated silk nanofibrous scaffold i.e., gelatin-permeated SF (in formic acid; T) exhibited highest ~770% gain from the initial dry weight. The likely reason behind high liquid gain % of gelatin-permeated SF (in formic acid; T) was due to hydrogel behaviour of gelatin present inside the porous structure of the scaffold. Non-treated SF (in aqueous; NT) started degrading after immersing in a PBS solution and degraded completely within 48 h in PBS.

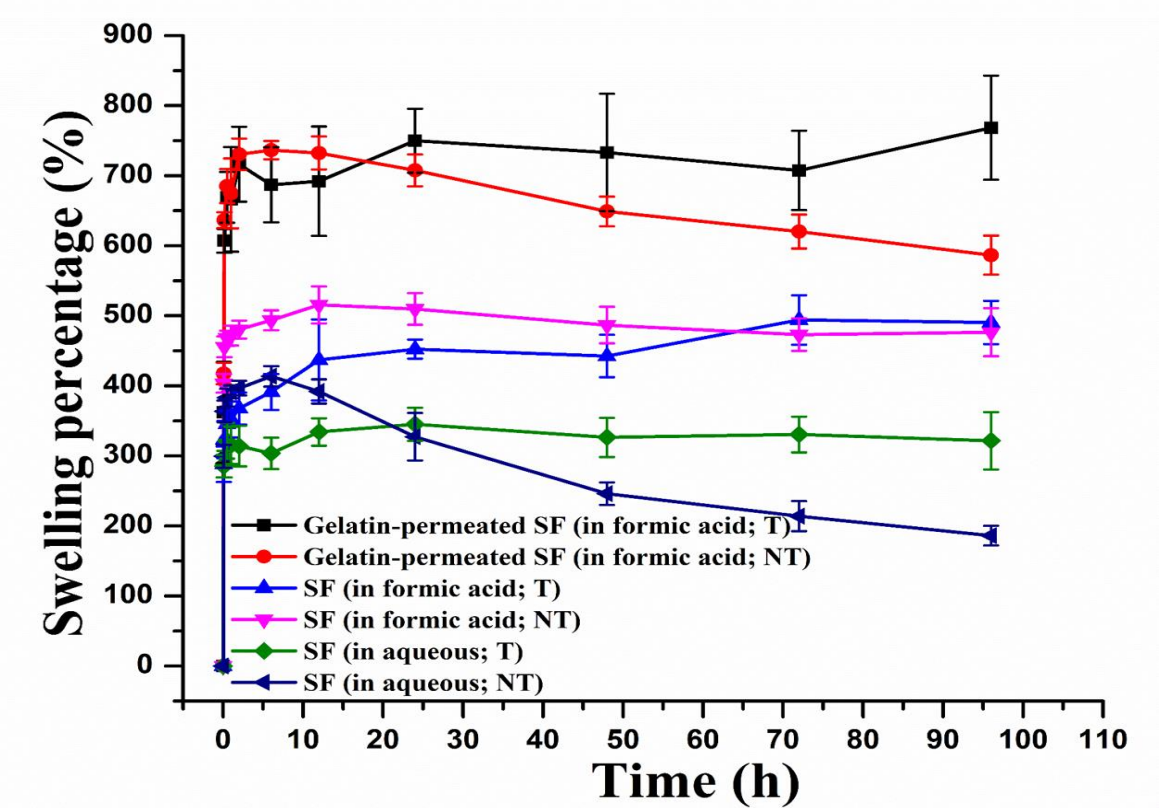

Figure 3.5 Graph shows weight gain percentage of ethanol treated samples namely, gelatin-permeated SF (in formic acid; T), SF (in formic acid; T), SF (in aqueous; T) and non-treated samples namely, gelatin-permeated SF (in formic acid; NT), SF (in formic acid; NT) and SF (in aqueous; NT).

3.3.1.5 Stability and degradation of electrospun nanofibers

The scaffolds were punched with a biopsy punch into discs of 10 mm diameter and soaked in PBS of pH 7.4 for 14 days at 37˚C. In figure 3.6 (a), digital images represent the nanofibrous sheets after 14 days incubation in PBS which shows no or little changes in their morphology except SF (in aqueous; NT) that degraded completely. All the samples except non-treated SF (in aqueous; NT) were found integrated enough to be held with forceps even after 14 days of incubation (Figure 3.6 (b)).

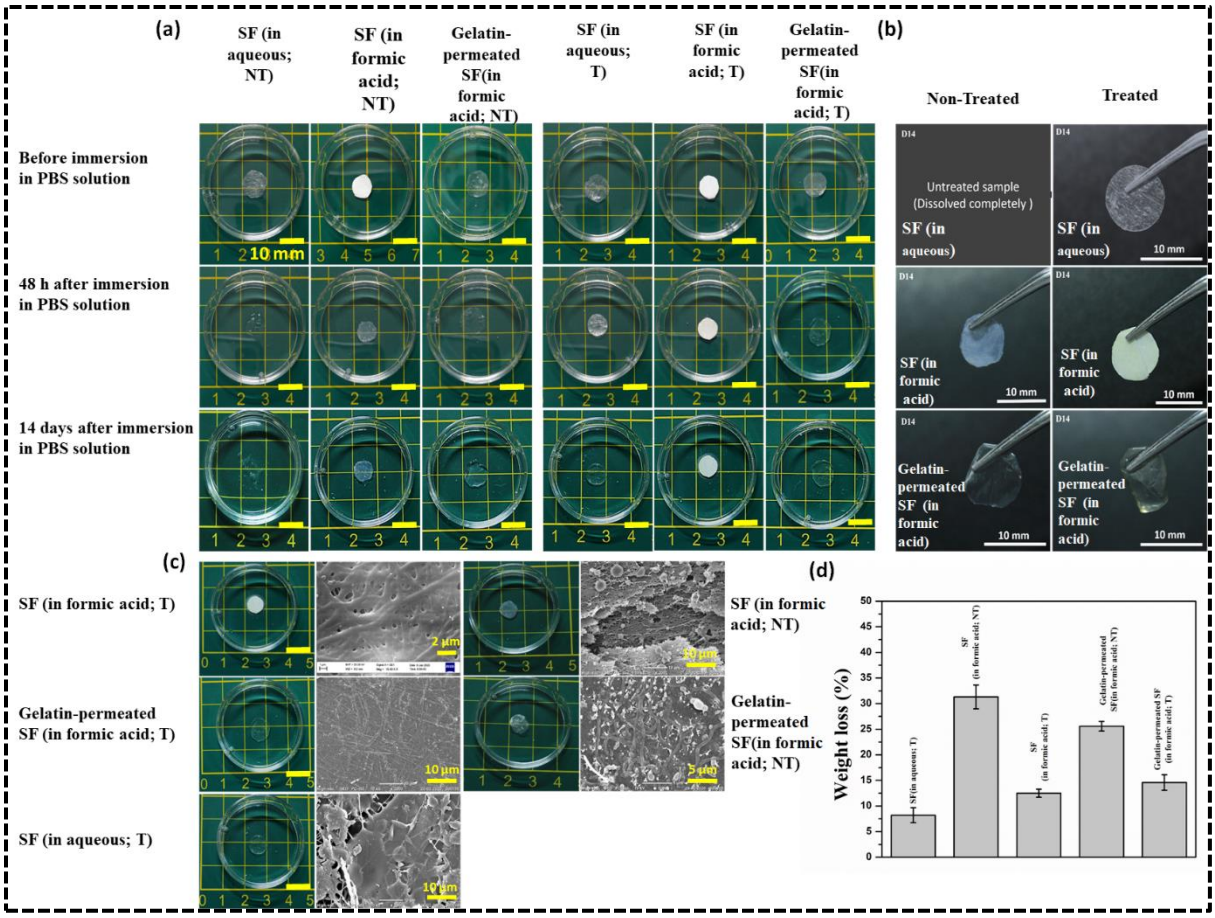

Figure 3.6 Depicts (a) digital images representing stability of prepared nanofibrous scaffolds in PBS at a room temperature (b) digital images of scaffolds held through forceps after 14 days immersed in PBS at 37˚C, (c) digital and SEM micrographs of electrospun samples after 14 days degradation in a lysozyme containing solution at 37˚C (d) graph shows weight loss percentage of samples over 14 days of immersion in a lysozyme containing solution at 37˚C. (Where NT= non-treated, T= ethanol treated).

Figure 3.6 (c) represents the digital images of scaffolds incubated in a lysozyme solution at a physiological temperature (37˚C). SF (in aqueous; NT) scaffold degraded almost completely within 48 h of incubation in a lysozyme solution at 37˚C. However, no clear deterioration was found when physically observed through digital images except SF (in aqueous; NT). SEM micrographs of the scaffolds depicted that all non-treated samples notably lost their fiber morphology up to high extent while the ethanol treated samples maintained their structural integrity and stability even after two weeks of incubation in the lysozyme solution at 37˚C. To

a very lesser extent, degradation on the exposed outer surface of the SF (in aqueous; T) was observed. SF (in formic acid; NT) scaffolds displayed a significant level of nanofibrous breakdown while SF (in formic acid; T) surface was negligibly affected as ethanol treatment stabilized the scaffold because of beta sheet formation within the silk nanofibers. Gelatin-permeated SF (in formic acid; NT) scaffolds represented partial degradation of both the polymers i.e., gelatin and silk. While, gelatin-permeated SF (in formic acid; T) scaffolds showed better integrity and least degradation because of physical crosslinking using ethanol. After 14 days of incubation of treated and non-treated samples, it was found that SF (in aqueous; NT), SF (in formic acid; NT) and gelatin-permeated SF (in formic acid; NT) showed 100%, 31.3 ± 2.3%, and 25.8 ± 1.0% weight loss, respectively, from the initial weight (Table 3.3). Whereas, SF (in aqueous; NT), SF (in formic acid; T) and gelatin-permeated SF (in formic acid; T) showed 8.2 ± 1.5%, 12.5 ± 0.8% and 14.6 ± 1.5% weight loss, respectively (Figure 3.6 (d)). The gelatin-permeated SF (in formic acid; T) exhibited a significant level of degradation because of its gelatin content which remains unaffected by ethanol treatment. It was concluded that ethanol vapor treatment provided better stability to the silk content, which ultimately enhanced the stability of fabricated scaffolds.

Table 3.3 Weight loss percentage of scaffolds after 14 days of incubation of treated and non-treated samples

Name of the Scaffold	Weight loss (%)
SF (In aqueous; T)	8.2 ± 1.5
SF (In formic acid; NT)	31.3 ± 2.3
SF (In formic acid; T)	12.5 ± 0.8
Gelatin-permeated SF (in formic acid; NT)	25.6 ± 1.0
Gelatin-permeated SF (in formic acid; T)	14.6 ± 1.6

3.3.1.6 Transparency measurement

Transparency measurement is an essential characteristic that must be considered while fabricating scaffolds related to corneal tissue engineering. The samples were scanned in the visible spectra (400-700 nm). SF (in aqueous; NT), SF (in formic acid; NT), gelatin-permeated SF (in formic acid; NT) scaffolds and their ethanol treated forms were scanned for their transparency using UV-Visible spectrophotometer. Furthermore, figure 3.7(a) represents the physical appearance of the scaffolds when placed on coloured number image with dark background; displaying similar trends as we observed using UV-Visible spectrophotometer. Figure 3.7(b) shows the physical appearance of ethanol treated scaffolds in PBS. The plotted graph shows that gelatin-permeated SF (in formic acid; NT) and its treated form gelatin-permeated SF (in formic acid; T) allow maximum visible light to pass through them (Figure 3.7 (c)). Transparency percentage of gelatin-permeated SF (in formic acid; NT) and gelatin-permeated SF (in formic acid; T) was observed to be 76.25-± 2.6% and 77.75 ± 2.3%, (scaffold thickness ~400-500 μm) respectively, with no significant difference observed in their transparency level even after ethanol treatment (Table 3.4). SF (in aqueous; T) hindered visible light little higher than gelatin-permeated SF (in formic acid; NT) and gelatin-permeated SF (in formic acid; T) resulting in transparency percentage around 67.5 ± 5.7% but slightly lower than SF (in aqueous; NT) (60.53 ± 5.6 %). SF (in formic acid; NT) depicted significantly low visible light transmission (46.5 ± 8.6%) while its treated form i.e., SF (in formic acid; T) absorbed majority of light and appeared opaque (1.2 ± 0.5%).

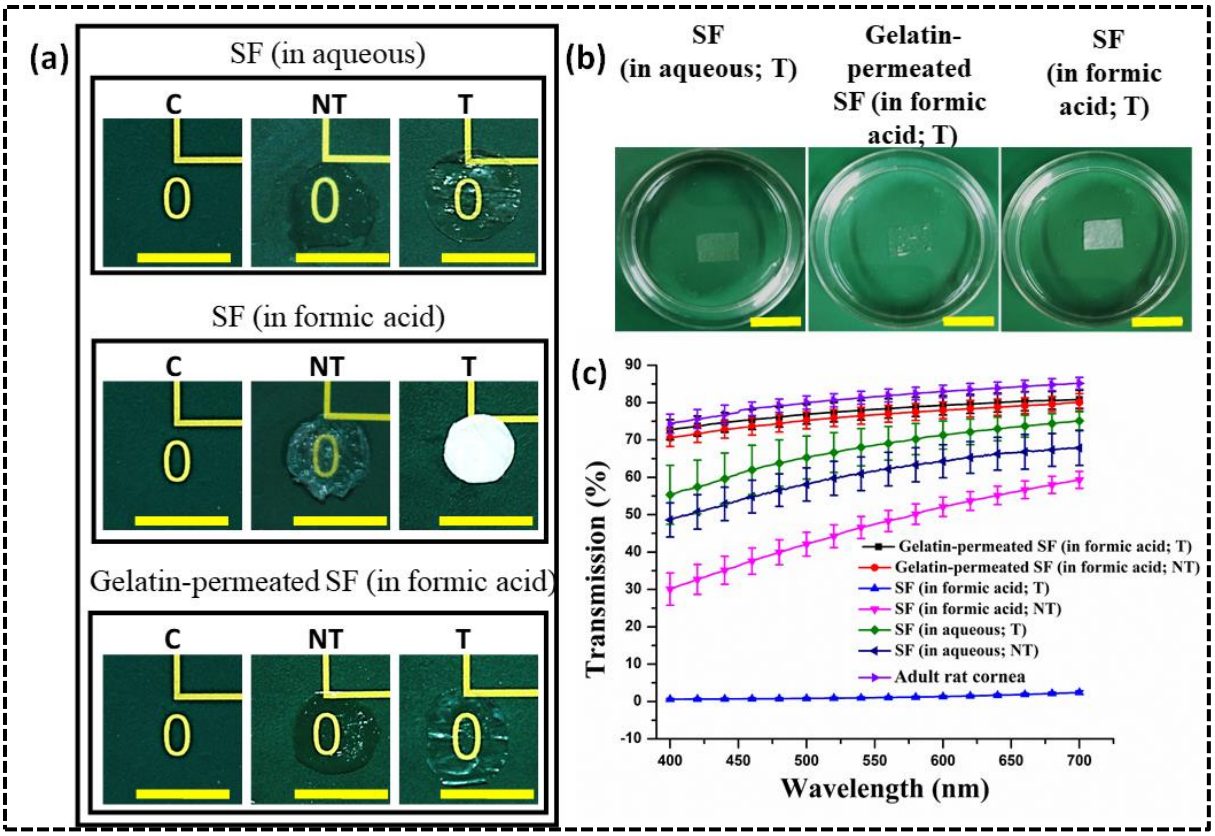

Figure 3.7 Transparency of adult rat cornea and different scaffolds namely SF (in aqueous), SF (in formic acid), gelatin-permeated SF (in formic acid) before (NT) and after ethanol vapor treatment (T) in PBS at a room temperature (25˚C) (a) digital images of samples showing visual transparency (b) shows the physical appearance of ethanol treated scaffolds in PBS and (c) graph shows percentage of light transmission through the samples. Scale bar: 10 mm. (where NT= non-treated, T= ethanol treated).

Table 3.4 Transparency percentage of the fabricated scaffolds quantified using UV-Visible spectrophotometer.

S.No.	Scaffold	Transparency (%)
1.	Gelatin-permeated SF (in formic acid; NT)	76.25 ± 2.6
2.	Gelatin-permeated SF (in formic acid; T)	77.75 ± 2.3
3.	SF (in aqueous; NT)	60.53 ± 5.6
4.	SF (in aqueous; T)	67.5 ± 5.7
5.	SF (in formic acid; NT)	46.5 ± 8.6
6.	SF (in formic acid; T)	1.2 ± 0.5

3.3.1.7 Contact angle measurement

The scaffolds were tested for their surface wetting behaviour to check the hydrophilic nature of the scaffold. Surface wettability usually involves the measurement of water contact angles. The contact angles of SF (in aqueous; NT), SF (in formic acid; NT) and gelatin-permeated SF (in formic acid; NT) were estimated around 67.29 ± 1.27, 43.01 ± 1.73 and 56.91± 1.16, respectively (Figure 3.8). Contact angles of treated samples were found significantly higher than their non-treated values. The contact angles for SF (in aqueous; T), SF (in formic acid; T) and gelatin-permeated SF (in formic acid; T) were 85.15 ± 2.08, 67.84 ± 1.42 and 78.00 ± 0.99, respectively. The bar graph and the digital images of the droplets on the scaffolds' surface signified the same. Studies suggest that, during transition from random coil to beta sheet conformation, silk fibroin may aggregate, crystallize and become dehydrated inducing the hydrophobicity on the silk surface (Ahmad et al. 2010; De Santis and Pantani 2013; Fan et al. 2012; Kishimoto et al. 2017).

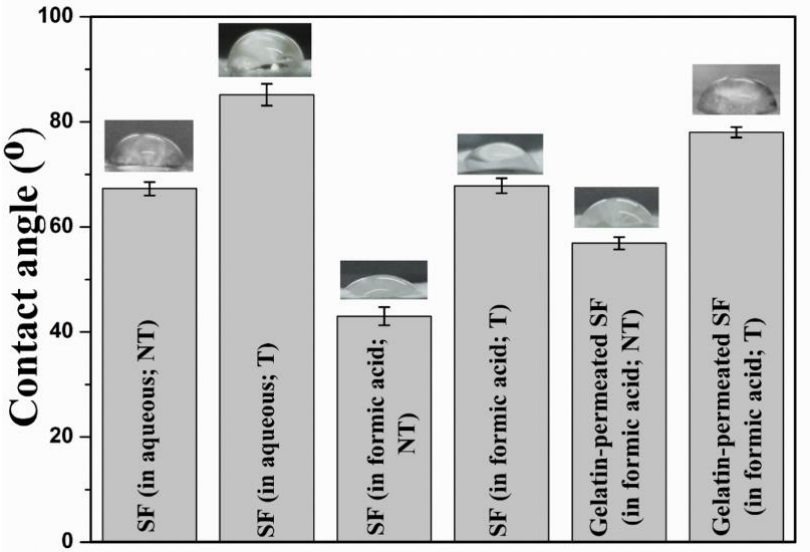

Figure 3.8 Represents the contact angles of non-treated SF (in aqueous; NT), SF (in formic acid; NT) and gelatin-permeated SF (in formic acid; NT) and their ethanol treated forms namely, SF (in aqueous; T), SF (in formic acid; T) and gelatin-permeated SF (in formic acid; T) indicating the wetting behaviour of scaffolds. (Where NT= non-treated, T= ethanol treated)

3.3.1.8 Mechanical testing of the scaffolds

Cornea acts as a wall to resist the intraocular pressure exerted by aqueous humor as well as vitreous humor fluids. Therefore, it is an indispensable feature to be considered while developing scaffolds for corneal tissue engineering. Human cornea has an elastic modulus of 0.579-4.9 MPa (Tonsomboon and Oyen 2013; Zeng et al. 2001). Characteristic strain-stress relationships for gelatin-permeated SF (in formic acid; T), gelatin-permeated SF (in formic acid; NT), SF (in aqueous; T), SF (in aqueous; NT), SF (in formic acid; T) and SF (in formic acid; NT) are shown in figure 3.9. Tensile strength and Young's modulus of gelatin-permeated SF (in formic acid; T), gelatin-permeated SF (in formic acid; NT), SF (in aqueous; T), SF (in aqueous; NT), SF (in formic acid; T) and SF (in formic acid; NT) nanofibrous scaffolds were found around 12.56 ± 0.69 MPa, 11.81 MPa, 7.11 ± 0.37 MPa, 6.38 ± 0.28 MPa, 9.12 ± 0.49 MPa and 6.53 ± 0.29 MPa, respectively (Figure 3.9). Gelatin permeation of electrospun silk nanofibrous scaffold i.e., gelatin-permeated SF (in formic acid; NT) resulted in an increase in its both tensile strength and young's modulus compared to SF (in aqueous; NT) and SF (in formic acid; NT). Moreover, scaffolds when treated with ethanol resulted in noticeably higher tensile strength and Young's modulus compared to that of non-treated samples. However, SF (in formic acid; NT) was found to have lowest tensile strength and Young's modulus that is most likely due to the high porosity. Results revealed that fabricated scaffolds exhibited comparatively higher elastic modulus than that of natural human cornea; thereby suggesting that the proposed scaffold would provide substantial mechanical stability for corneal tissue fabrication.

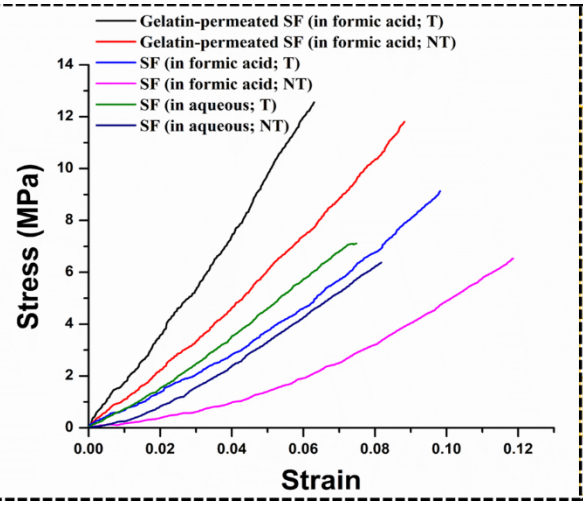

Sample	Tensile Strength (MPa)	Young's Modulus (MPa)
Gelatin-permeated SF (in formic acid; T)	12.56 ± 0.69	175 ± 0.69
Gelatin-permeated SF (in formic acid; NT)	11.81 ± 0.55	124 ± 1.70
SF (in aqueous; T)	7.11 ± 0.37	82.34 ± 0.33
SF (in aqueous; NT)	6.53 ± 0.28	32.14 ± 0.53
SF (in formic acid; T)	9.12 ± 0.49	90.79 ± 0.54
SF (in formic acid; NT)	6.38 ± 0.29	22.01 ± 0.16

Figure 3.9 Depicts the tensile stress-strain curve of non-treated SF (in aqueous; NT), SF (in formic acid; NT) and gelatin-permeated SF (in formic acid; NT) and their ethanol treated forms namely, SF (in aqueous; T), SF (in formic acid; T) and gelatin-permeated SF (in formic acid; T) indicating the mechanical stability of respective scaffolds. (Where NT= non-treated, T= ethanol treated).

3.3.1.9 Cellular compatibility

Figure 3.10 illustrates the microscopic images of SIRC (rabbit corneal fibroblast) and L929-RFP (mouse skin fibroblast) cells cultured within the prepared nanofibrous scaffolds for 2, 4 and 6 days. Cells cultured on the fabricated scaffolds were performed to evaluate the cytocompatibility of the scaffolds. Cells were cultured on treated SF (in aqueous; T) and gelatin-permeated SF (in formic acid; T) scaffolds as these were the scaffolds that showed maximum transparency compared to the transparency of other scaffolds. Both cells types exhibited better cellular biocompatibility as well as the optimal level of proliferation. The cytocompatibility of cells in the gelatin-permeated SF (in formic acid; T) was significantly higher compared to that of SF (in aqueous; T) scaffolds. The possible reason may be because of good wettability and the presence of collagen equivalent (e.g. gelatin). No significant compromise in the physical stability and integrity of the scaffolds was noticed in the Petri dish until 6 days of cell culture.

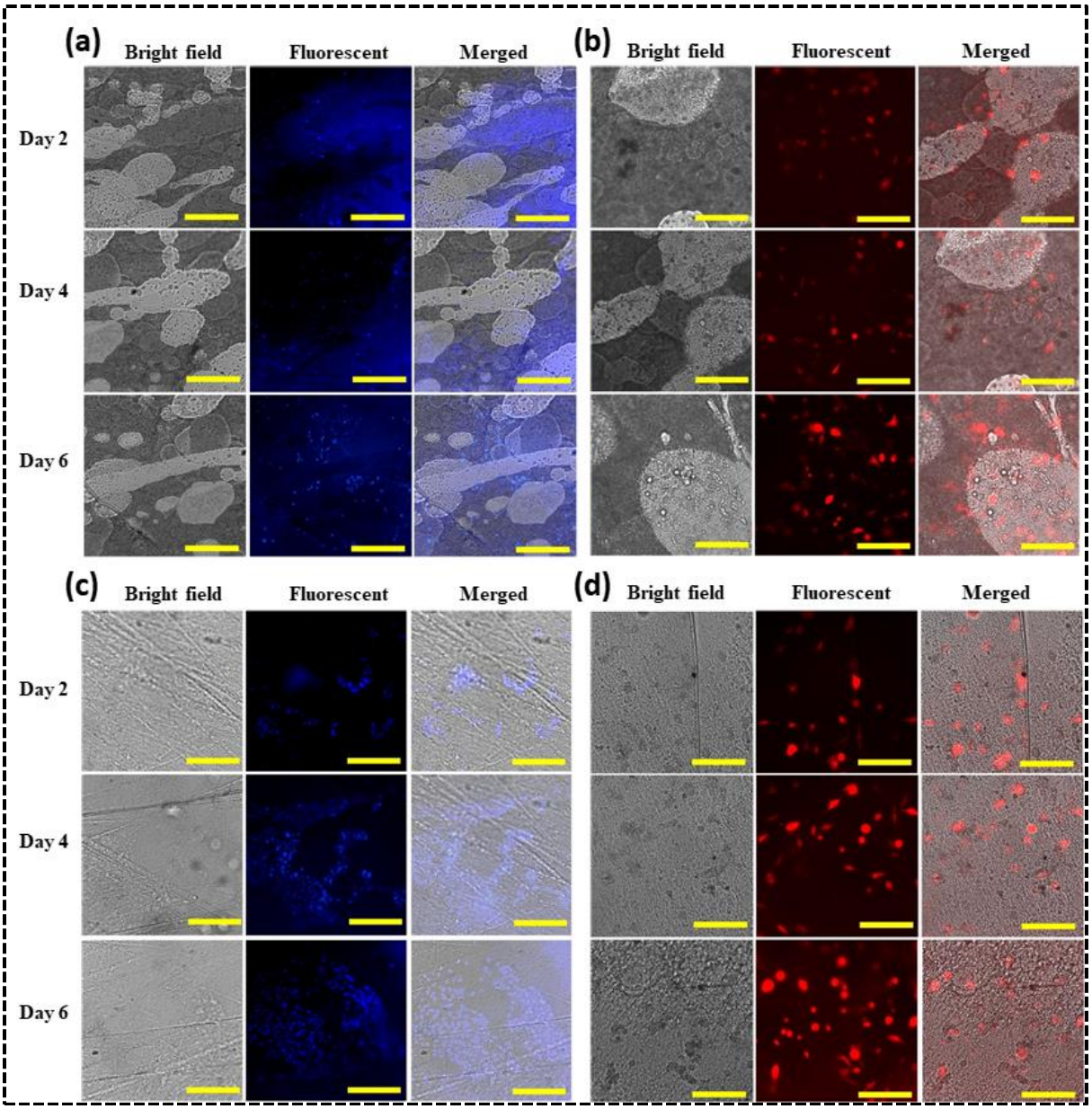

Figure 3.10 The above panel of images represents the cells cultured within the ethanol treated SF (in aqueous; T) scaffold using (a) corneal fibroblast SIRC cells (DAPI staining) and (b) L929-RFP fibroblast cells for over a period of 6 days. (c) Represents SIRC cells (DAPI staining) cultured on gelatin-permeated SF (in formic acid; T) and (d) L929-RFP cells cultured on gelatin-permeated SF (in formic acid; T) scaffolds for over a period of 6 days. Scale bar is 100 µm for bright field, fluorescent and merged images. (Where NT= non-treated, T= ethanol treated).

3.3.1.10 MTT Assay

A significant enhancement in the cellular viability was observed over a period of 6 days culture on the SF (in aqueous; T) and gelatin-permeated SF (in formic acid; T) scaffolds for both SIRC cells and L929-RFP cells (Figure 3.11). SF (in aqueous; T) scaffolds showed a noticeable increase in the proliferation percentage of SIRC cells from 15.99± 1.63 % on 2^{nd} day to 38.74 ± 2.36 % by 4^{th} day and 69.44 ± 1.67 % by 6^{th} day with respect to 6^{th} day control for (SIRC) fibroblast cells cultured in Petri dishes (Figure 3.11 (a)). For L929-RFP, SF (in aqueous; T) showed cellular proliferation from 16.28 ± 0.56% on 2^{nd} day followed by 41.79 ± 1.15% and 70.51 ± 3.05% on 4^{th} and 6^{th} day, respectively, with respect to 6^{th} day control for (L929-RFP) fibroblast cell cultured in Petri dishes (Figure 3.11 (b)). Gelatin-permeated SF (in formic acid; T) scaffolds displayed a significant increase in the percentage of SIRC cellular proliferation from 19.11 ± 2.40% on 2^{nd} day to 45.88 ± 1.57% by 4^{th} day and to 75.26 ± 1.89% by 6^{th} day with respect to 6^{th} day control for (SIRC) fibroblast cell cultured in Petri dishes (Figure 3.11 (a)). Furthermore, gelatin-permeated SF (in formic acid; T) scaffolds exhibited a noted increase in cellular proliferation of L929-RFP cells from 20.20 ± 1.09% on 2^{nd} day followed by 48.49 ± 1.43% and 77.37 ± 2.24% on 4^{th} and 6^{th} day, respectively, with respect to 6^{th} day control for (L929-RFP) fibroblast cell cultured in Petri dishes (Figure 3.11 (b)). Figure 11 (c) shows a comparative cell proliferation percentage of cells cultured on SF (in aqueous; T) and gelatin-permeated SF (in formic acid; T) scaffolds. Addition of gelatin to the silk nanofibrous scaffold improved the cellular biocompatibility and proliferation of mammalian cells by providing high cell adhesive moieties. The inclusion of gelatin in gelatin-permeated SF (in formic acid; T) has resulted in much improved cellular biocompatibility compared to SF (in aqueous; T), which is most likely due to the presence of gelatin.

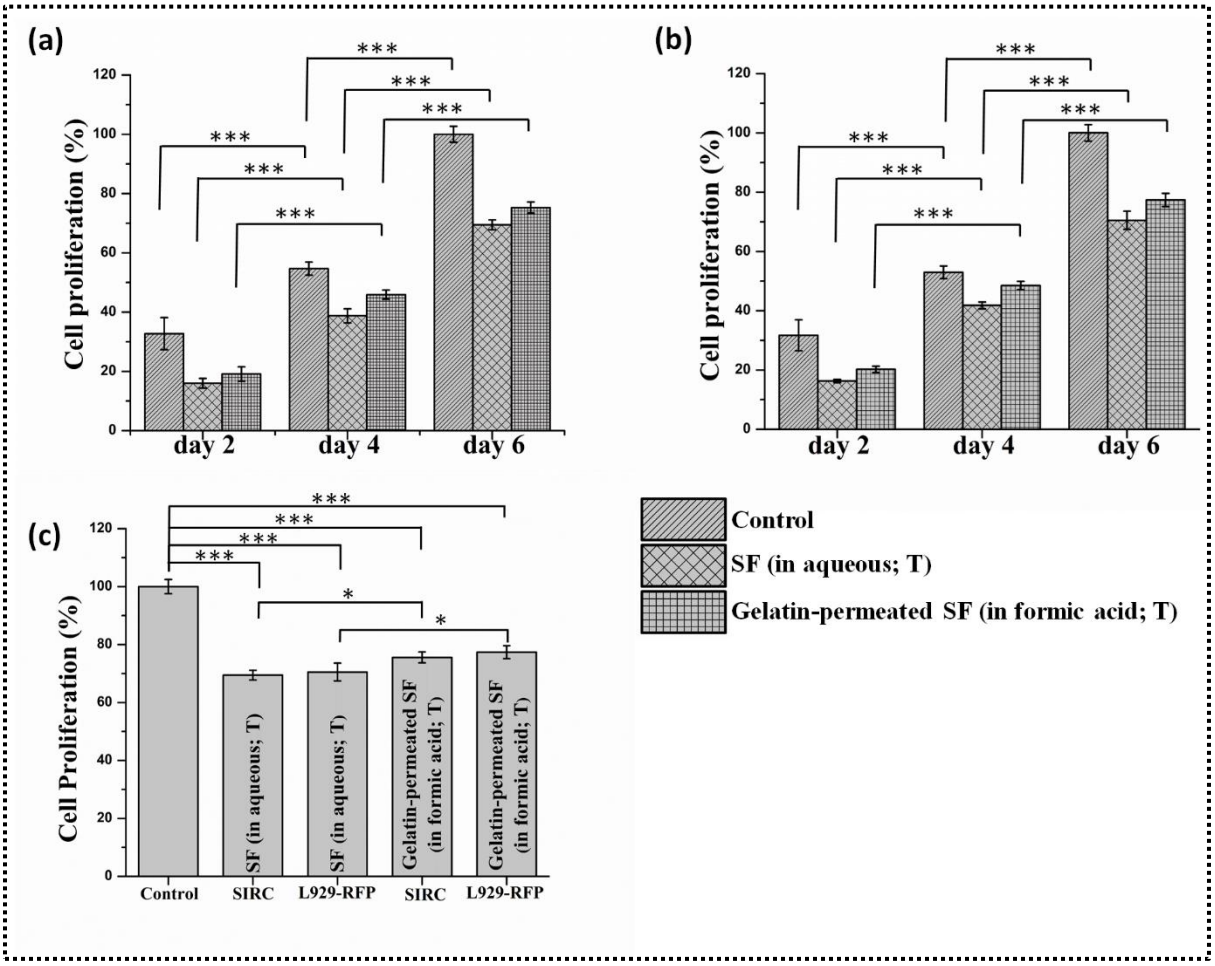

Figure 3.11 The figure illustrates the percentage cellular viability of (a) SIRC cells (b) L929-RFP cells for 2, 4 and 6 days and the cytocompatibility of the scaffolds as determined by MTT assay (c) comparative cell proliferation percentage values of cells cultured on SF (in aqueous; T) and gelatin-permeated SF (in formic acid; T) scaffolds. In this experiment, absorbance for the 6th day culture of positive control was considered as reference OD for all the samples. Values are expressed as mean ± SD ($n = 3$) and the level of significance as ***$p < 0.05$. (Where NT= non-treated, T= ethanol treated).

3.4 Discussion

The objective of this chapter was to fabricate and examine the nanofibrous silk-gelatin composite scaffolds for corneal tissue engineering applications. Several factors such as stiffness of material, cellular behaviour towards mechanical properties of scaffolds, scaffold

permeability to allow nutrients and gasses into the central region and transparency need to be considered while fabricating corneal scaffolds (Ahearne et al.,.; Kong et al. 2017; Lynch, Wilson, and Ahearne 2016; Matthyssen et al. 2018; Tonsomboon and Oyen 2013). We have implemented electrospinning approach to fabricate the scaffolds; since many researchers have reported about the virtue of electrospinning to forge scaffolds for corneal tissue engineering (Ahearne et al.,; Aldana and Abraham 2017; Hashimoto et al. 2010; Ibrahim, Kakarougkas, and Allam 2017; Li and Xia 2004; Mohammadzadehmoghadam and Dong 2019).

Various natural and synthetic biomaterials have been exploited to develop stromal equivalents; in particular, Acun et al. have developed foam based collagen scaffolds that demonstrated good transparency, however utilized toxic chemical crosslinkers; that exhibited limited mechanical strength and delivered relatively expensive scaffolds (Acun and Hasirci 2014). Biazar et al. have fabricated silk nanofibrous scaffolds that showed adequate corneal fibroblast interaction and sufficient mechanical properties (Biazar et al. 2015). Moreover, Tonsomboon et al. proclaimed aligned electrospun gelatin-alginate composite nanofibrous scaffolds exhibiting comparable mechanical strength of cornea. However, reports revealed usage of toxic chemical crosslinker to stabilize the scaffold. Also, cellular interaction with the scaffolds was found lacking in the proposed scaffolds (Tonsomboon and Oyen 2013). Recently, Hazra et al. utilized silk film to reveal the transparency and its interaction with corneal epithelial cells, however, the proposed film based scaffold still remained to be analyzed for its mechanical strength, porosity and behaviour towards corneal fibroblast cells (Hazra et al. 2016).

Gelatin is an inexpensive hydrolyzed component of collagen, which constitutes the major protein of extracellular matrix and is considered to be a biodegradable, biocompatible and non-immunogenic natural polymer for clinical applications (Aldana and Abraham 2017; Babitha et

al. 2017). However, it has a few limitations such as inferior mechanical properties, fast degradation rate and low thermal stability. To overcome these limitations, researchers have developed gelatin-based composites (Echave et al. 2017). On the other hand, silk has been well known for its transparency and mechanical strength which are the major essential features required for corneal tissue engineering; however, due to lack of bioactive peptides it is unable to support cell and other biological activities as satisfactorily as other proteins like collagen and gelatin and also has low biodegradability (Buitrago et al. 2018). Both polymers (i.e., silk and gelatin) are derived from natural resources that enable them for biocompatibility and low cost. Therefore, composites and blends of silk and gelatin have been explored by some researchers to synergize their properties and validate their efficacy for various tissue engineering applications (Okhawilai et al. 2010; Taddei et al. 2013; Mohammadzadehmoghadam and Dong 2019; Gui-Bo et al. 2009); however, very few work have made attempts to explore silk-gelatin composites for corneal tissue engineering applications (Sahi et al. 2020; Farasatkia et al. 2021). This motivated us to explore the composite of gelatin and silk fibroin for the development of corneal stromal constructs.

Fabrication of electrospun silk using formic acid solvent exhibits even nanofibers with adequate porosity; however, usage of formic acid enables desiccated, brittle and least transparent scaffold (Gandhi et al. 2009; Cho et al. 2014; Freddi et al. 1995). Therefore, silk-gelatin blend and composite based scaffolds have gained recognition (Cho et al. 2014). Addition of gelatin to silk provides improved mechanical properties compared to silk alone (Mohammadzadehmoghadam and Dong 2019; Okhawilai et al. 2010). However, light transmission percentage of silk/gelatin blend based scaffolds reported in the literature remains to be fully explored. Farasatkia et al. attempted to fabricate transparent hybrid films based on

silk nanofibrils (SNF)/gelatin methacryloyl (GelMA). Although the fabricated scaffold exhibited some promising approach in terms of mechanical stability and transparency, usage of GelMA compels it as an expensive outcome (Farasatkia et al. 2021).

In addition, we attempted to perform electrospinning of silk fibroin in its aqueous state. However, silk alone is difficult to draw into nanofibrous scaffold since there are certain governing factors such as viscosity, surface tension, critical concentration and applied voltage; and the SF (in aqueous) has limitation to surpass these factors without any additive (Cao et al. 2009; Kishimoto et al. 2017; Min et al. 2004). Study suggests that the surface tension of the aqueous silk is relatively higher compared to that of the one prepared in formic acid (Haider, Haider, and Kang 2018; Qi et al. 2017); therefore, selecting formic acid as a solvent for silk would reduce surface tension that favours Taylor cone generation and jet fiber forming capability which results in fabrication of electrospun nanofibers (Koeppel, Laity, and Holland 2018; Yao et al. 2003). Although there are few reports where aqueous silk alone is used to be drawn into nanofibers through adjusting the voltage applied, the resulting nanofibers are found to have diameter in the range of 700-800 nm which is unacceptable in case of fabrication of corneal tissue scaffolds (Cao et al. 2009; Kishimoto et al. 2017; 2018; Wang et al. 2004). Changing the solvent to formic acid thus helps reducing the surface tension that favours the electrospinning process and thus the nanofibers with expected properties can be obtained. Nanofibrous scaffolds fabricated using electrospinning methodology exhibit close structural resemblance with native ECM of cornea and possess high surface area-to- volume ratio and excellent porosity, which facilitate cellular adhesion, migration, proliferation, suturability and good mechanical strength. Scanning electron microscopy (SEM) images depict similar nanofibrous structures with majority of fibers in a partially aligned manner with fiber diameter

ranging from 40-320 nm, which is close to the diameter of a pair of native collagen fibers of cornea (average diameter of corneal collagen is ~25-34 nm) (Komai and Ushiki 1991; Meek 2009; Tonsomboon and Oyen 2013). Fiber diameter tunability feature could be utilized to fabricate nanofibers similar to native collagen, that would ultimately enhance the transparency of the scaffold alike native cornea (Babitha et al. 2017; Baradaran-Rafii, Biazar, and Heidari-Keshel 2015; Kong and Mi 2016; Ye et al. 2014; Zhao et al. 2015).

Cellular permeability is another factor that cannot be overlooked while designing corneal scaffold as it is vital for allowing gasses and nutrients to the central part of cornea (Ahearne et al.,; Edwards and Prausnitz 1998; Murphy, Haugh, and O'Brien 2010). As per the SEM image data, porosity of SF (in formic acid; NT) nanofibrous scaffold was found to be 47.30 ± 0.90% of the total area while it was difficult to determine the porosity of SF (in aqueous; NT) and gelatin-permeated SF (in formic acid; NT). Since the entire three-dimensional (3D) network of gelatin-permeated SF (in formic acid; NT) was already occupied with permeated gelatin, there was no significant level of porosity observed as obtained using ImageJ. Moreover, it is anticipated that the gelatin would assist as a cell adhesion material in gelatin-permeated SF (in formic acid) and degrade eventually leaving behind the porous structure for further cellular growth, migration and proliferation (Ahearne et al.,; Echave et al. 2017; Rose et al. 2014; Sun et al. 2018).

ATR-FTIR of the scaffolds confirms the characteristic peaks of the polymeric materials. Gelatin-permeated SF (in formic acid; NT) reveals the presence of both the polymers i.e., silk and gelatin. Ethanol vapor treatment shifted major silk characteristic peaks from random coil arrangement (silk I) to beta sheet conformation (silk II), resulting in better stability (Amiraliyan, Nouri, and Haghighat Kish 2010; Shen et al. 2015). Gelatin remains unaffected

from ethanol vapor treatment. Water content of the ethanol vapor (70% v/v) during its treatment expands the amorphous region of the protein owing to the interruption of hydrogen bonds followed by ethanol penetration in the expanded region generating hydrophobic environment (Min et al. 2006; Cao et al. 2009; Qi et al. 2017). Furthermore, the hydrophobic molecules chain segment in the random coil accumulates closely forming crystal nucleus. Moreover, growth in crystal nucleus and rearrangement of hydrogen bonds result in a stable beta sheet conformation (Hu, Kaplan, and Cebe 2006; Min et al. 2004; 2006; Qi et al. 2017). Hydrogen bond rearrangement leads to water loss and creates more stable beta sheets that result into shrinkage of nanofibrous structure followed by a noted increase in hydrophobic characteristics leading to enhanced contact angles (Yusoff et al. 2019). Once they form beta sheet crystal like structure, the scaffolds become brittle and less transparent and such outcomes are reported in the previous literatures (Jin et al. 2005; Minoura, Tsukada, and Nagura 1990; Qi et al. 2017). In the present study, gelatin infiltration inside the silk nanofibrous structure however resisted transparency loss and brittleness of the fabricated scaffold.

Transparency, being the most essential characteristic of the fabricated scaffolds, was estimated. There are numerous reports stating the corneal transparency around 80% in the visible range of wavelengths of light (Ahearne et al.,; Doutch et al. 2008; Freegard 1997; Hashimoto et al. 2010; Qazi et al. 2010). Gelatin-permeated SF (in formic acid; NT) and gelatin-permeated SF (in formic acid; T) has shown maximum transparency significantly comparable to that of native cornea (Hashimoto et al. 2010). Percentage light transmission of SF (in aqueous; T) was found significantly lower than that of gelatin-permeated SF (in formic acid; NT) and gelatin-permeated SF (in formic acid; T); however, noticeably higher than the transparency level of SF (in aqueous; NT). SF (in formic acid; NT) nanofibrous scaffold showed transparency

significantly lower than gelatin-permeated SF (in formic acid; NT), Gelatin-permeated SF (in formic acid; T) and SF (in aqueous; T). SF (in formic acid; NT) scaffold turned opaque on ethanol vapor treatment and showed minimum percentage of light transmission; rendering them difficult to be used for corneal tissue engineering. Gelatin permeation has occupied the porous space of silk nanofibers allowing a continuous uninterrupted path (with least diffraction) for visible light enabling it transparent, comparable to that of cornea (Nogi et al. 2009; Ifuku et al. 2013). Furthermore, gelatin permeation inside silk nanofibrous cavities has delivered a film like substrate facilitating for cellular adhesion and proliferation.

Although silk/gelatin blends have shown profound mechanical stability, transparency plays a crucial role while developing scaffolds for cornea (Taddei et al. 2013; Farasatkia et al. 2021; Okhawilai et al. 2010). In addition, we also analyzed the transparency of silk/gelatin blend (SF/G blend (in formic acid)) nanofibers and the obtained values were found to be quite low in comparison to that of native cornea (Figure 3.12). The best persuasive reason regarding low light transmission through the nanofibrous silk/gelatin blend might be the presence of microporous structures as void spaces in the sheet that possibly led to high visible light scattering. Moreover, the ethanol crosslinking significantly reduced the transparency of the nanofibrous scaffold. Water contact angles of all the ethanol treated and non-treated samples were examined to determine the hydrophilicity of the fabricated scaffolds. The contact angles for ethanol vapor treated samples were found significantly increased compared to non-treated samples because of modification of random coil conformation to beta sheets inside the silk, present in the scaffolds. All the scaffolds were showing variable contact angles depending upon their hydrophilic properties. SF (in aqueous; T) showed maximum contact angle (85.15 ± 2.08)

compared to other scaffolds; whereas, SF (in formic acid; NT) nanofibrous scaffold exhibited minimum contact angle (43.01 ± 1.73) because of high porosity of the scaffold.

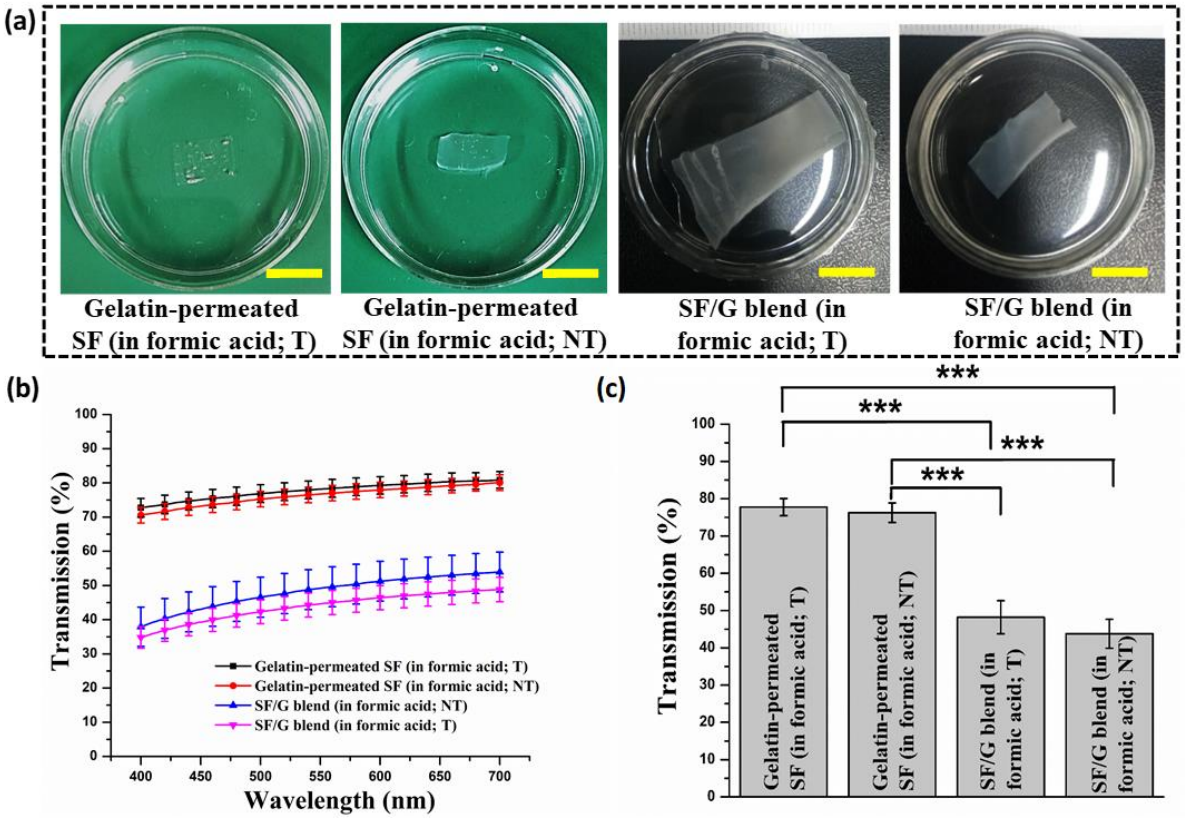

Figure 3.12 Represents (a) digital images of gelatin-permeated SF (in formic acid) and silk-gelatin blend (SF/G blend (in formic acid)) placed in PBS showing visual transparency [scale bar = 10 mm] (b) Transparency of gelatin-permeated SF (in formic acid) composite and SF/G blend (in formic acid) scaffolds before (NT) and after ethanol vapor treatment (T) in PBS at a room temperature (25˚C) and (c) Their comparative bar graph displaying low level of transparency for SF/G blend (in formic acid) compared to gelatin-permeated SF (in formic acid) composite. (Where NT= non-treated, T= ethanol treated)

Gelatin-permeated SF (in formic acid; NT) and gelatin-permeated SF (in formic acid; T) illustrated contact angles notably higher than SF (in formic acid; NT) most likely due to permeation of their porous spaces with gelatin. Moreover, cell proliferation on gelatin-permeated SF (in formic acid; T) scaffolds were observed remarkably better than those of other scaffolds because of the presence of gelatin and hydrophilic behavior.

Water retention capacity of gelatin-permeated SF (in formic acid; T) was found significantly highest (i.e., ~700%) among all the three scaffolds fabricated, most likely due to the hydrophilic behaviour of gelatin. The liquid retention capacity of SF (in formic acid; T) and SF (in aqueous; T) was observed almost similar ranging ~450% and ~300%, respectively. Lowest water retention capacity of SF (in aqueous; T) could be attributed to their least porosity within the scaffold. Optimal water retention capacity is very much essential for a standard scaffold to facilitate smooth supply of nutrients to each and every part of the scaffold; therefore, high liquid retention capacity of gelatin-permeated SF (in formic acid; T) enables them as a better scaffold for corneal tissue engineering. In addition, all the scaffolds incubated in PBS showed remarkable stability except SF (in aqueous; NT) which degraded almost completely within 48 h of incubation. Degradation of the scaffolds was also studied in a lysozyme containing solution to mimic the physiological environment and to test stability of the scaffolds. Gelatin-permeated SF (in formic acid; T) underwent through a significant level of degradation compared to SF (in aqueous; T) after 14 days of incubation in a lysozyme-containing solution; signifying an essential feature of the optimal scaffold (Ahearne et al.; Kong and Mi 2016; Matthyssen et al. 2018). The most likely reason for gelatin-permeated SF (in formic acid; T) degradation could be the degradation of its gelatin content during incubation, which is not cross-linked in the present study and therefore its gradual loss helps exposing the inner silk nanofibers. Degradation of gelatin would expose the pores inside the silk nanofibers that would lead to migration and proliferation of cells inside the nanofibrous structure, whereas the silk nanofibers would provide the integrity and the mechanical stability to the scaffold. Although SF (in aqueous; T) is highly stable to degradation due to the

unavailability of pores inside the scaffolds; it could be beneficial for the applications where cellular proliferation is required on the surface only.

Tensile strength of gelatin-permeated SF (in formic acid; T) was found highest around 12.56 MPa compared to gelatin-permeated SF (in formic acid; NT) i.e., 11.81 MPa. Similarly, Young's modulus followed similar trend and was found around ~175 MPa and ~124 MPa for gelatin-permeated SF (in formic acid; T) and gelatin-permeated SF (in formic acid; NT) respectively. Ethanol vapor treatment also enhanced the mechanical strength of the scaffolds. The possible reason for the enhanced mechanical properties of ethanol treated samples could be attributed to the increased beta sheet formation in silk fibroin due to ethanol treatment, which was confirmed by ATR-FTIR analysis (Varshney et al. 2020; Sahi et al. 2020). Reported study indicates that the addition of gelatin enhances the crosslinking property of the scaffold and ultimately the strength of the modified scaffolds (Mohammadzadehmoghadam and Dong 2019). Although permeation of gelatin content reduces the flexibility, the strength and cellular biocompatibility of the scaffold are significantly enhanced. Overall, tensile strength and Young's modulus values of all the fabricated scaffolds were found noticeably higher than that of the native cornea (i.e., 0.579-4.9 MPa), suggesting its potential to be utilized for corneal tissue engineering (Zeng et al. 2001; Tonsomboon and Oyen 2013).

MTT and cell culture results show that the addition of gelatin to the silk nanofibrous scaffold improves the cellular biocompatibility and proliferation of mammalian cells by providing high cell adhesive moieties. Gelatin-permeated SF (in formic acid; T) has shown noticeably better cellular growth compared to SF (in aqueous; T) most likely due to the presence of gelatin. Since SF (in formic acid) turned opaque upon ethanol treatment, their cellular biocompatibility has not further been studied. Cellular proliferation of L929-RFP cells was found slightly higher

than that of SIRC cell lines for all the scaffolds tested. Physical crosslinking of silk using ethanol vapor treatment resulted in better stability without any chemical or enzymatic crosslinker. Gelatin content inside the scaffold played an important role in the regulation of cellular functions. Overall, our results suggested that addition of gelatin to SF (in formic acid) nanofibers resulted in a superior scaffold i.e., gelatin-permeated SF (in formic acid; T) that exhibited enhanced transparency, stability and cellular cytocompatibility. Therefore, the formation of the biocompatible scaffolds based on silk and gelatin is pivotal and forms the basis of future research and advancement towards corneal tissue engineering.

3.5 Conclusion

A novel nanocomposite gelatin hydrogel system reinforced with mechanically strong silk nanofibers was successfully developed. Permeation of gelatin inside silk nanofibrous scaffold resulted in an enhanced percentage of light transmission in the visible range which increased its utility in various applications where transparency plays a major role such as skin wound dressing and most importantly in corneal tissue constructs. Ethanol vapor treatment of the silk-based scaffolds led to conversion of less stable random helical conformation to a more stable β sheets conformation in silk nanofibers. Liquid retention capacity of gelatin-permeated SF (in formic acid; T) was found notably highest compared to those of SF (in aqueous; T) and SF (in formic acid; T). All the scaffolds were stable upto 2 weeks of incubation in either PBS or lysozyme containing PBS solution without any change in the physical appearace except SF (in aqueous; NT). Degradation study revealed improved and better stability for all the ethanol treated samples. Cytocompatibility of both corneal fibroblast SIRC cells and L929-RFP fibroblast cells was found remarkably better in gelatin-permeated SF (in formic acid; T) scaffold compared to the other scaffolds. Novelty of the present work is the development of

nanofibrous silk-gelatin composite scaffolds imparting optimal transparency, improved mechanical strength and better cellular biocompatibility compared to other reported studies. Overall, the outcomes revealed that addition of gelatin in the nanofibrous silk scaffolds resulted in stable, highly cytocompatible and transparent scaffolds that render them as an appropriate candidate for corneal tissue engineering. Although in vitro characterization of the material has been successfully demonstrated in the present study, further intensive in vivo characterization is required to validate the proposed materials useful for developing corneal stromal equivalents.

3.6 References

Acun, A., and V. Hasirci. 2014. "Construction of a Collagen-Based, Split-Thickness Cornea Substitute." *Journal of Biomaterials Science, Polymer Edition* 25 (11): 1110–32. https://doi.org/10.1080/09205063.2014.920170.

Ahearne, Mark, Julia Fernández-Pérez, Sophia Masterton, Peter W. Madden, and Promita Bhattacharjee. 2020 "Designing Scaffolds for Corneal Regeneration." *Advanced Functional Materials* n/a (n/a): 1908996. https://doi.org/10.1002/adfm.201908996.

Ahmad, Zubair, K. Dinesh Kumar, Madhumita Saroop, Nisha Preschilla, Amit Biswas, Jayesh R. Bellare, and Anil K. Bhowmick. 2010. "Highly Transparent Thermoplastic Elastomer from Isotactic Polypropylene and Styrene/Ethylene-Butylene/Styrene Triblock Copolymer: Structure-Property Correlations." *Polymer Engineering & Science* 50 (2): 331–41. https://doi.org/10.1002/pen.21540.

Aldana, Ana A., and Gustavo A. Abraham. 2017. "Current Advances in Electrospun Gelatin-Based Scaffolds for Tissue Engineering Applications." *International Journal of Pharmaceutics* 523 (2): 441–53. https://doi.org/10.1016/j.ijpharm.2016.09.044.

Amiraliyan, N., M. Nouri, and M. Haghighat Kish. 2010. “Structural Characterization and Mechanical Properties of Electrospun Silk Fibroin Nanofiber Mats.” *Polymer Science Series A* 52 (4): 407–12. https://doi.org/10.1134/S0965545X10040097.

Babitha, S., Lakra Rachita, K. Karthikeyan, Ekambaram Shoba, Indrakumar Janani, Balan Poornima, and K. Purna Sai. 2017. “Electrospun Protein Nanofibers in Healthcare: A Review.” *International Journal of Pharmaceutics* 523 (1): 52–90. https://doi.org/10.1016/j.ijpharm.2017.03.013.

Baradaran-Rafii, Alireza, Esmaeil Biazar, and Saeed Heidari-Keshel. 2015. “Cellular Response of Limbal Stem Cells on PHBV/Gelatin Nanofibrous Scaffold for Ocular Epithelial Regeneration.” *International Journal of Polymeric Materials and Polymeric Biomaterials* 64 (17): 879–87. https://doi.org/10.1080/00914037.2015.1030658.

Beems, E. M., and J. A. Van Best. 1990. “Light Transmission of the Cornea in Whole Human Eyes.” *Experimental Eye Research* 50 (4): 393–95. https://doi.org/10.1016/0014-4835(90)90140-p.

Biazar, Esmaeil, Alireza Baradaran-Rafii, Saeed Heidari-keshel, and Sara Tavakolifard. 2015. “Oriented Nanofibrous Silk as a Natural Scaffold for Ocular Epithelial Regeneration.” *Journal of Biomaterials Science. Polymer Edition* 26 (16): 1139–51. https://doi.org/10.1080/09205063.2015.1078930.

Buitrago, Jennifer O., Kapil D. Patel, Ahmed El-Fiqi, Jung-Hwan Lee, Banani Kundu, Hae-Hyoung Lee, and Hae-Won Kim. 2018. “Silk Fibroin/Collagen Protein Hybrid Cell-Encapsulating Hydrogels with Tunable Gelation and Improved Physical and Biological Properties.” *Acta Biomaterialia* 69: 218–33. https://doi.org/10.1016/j.actbio.2017.12.026.

Cao, Hui, Xin Chen, Lei Huang, and Zhengzhong Shao. 2009. “Electrospinning of Reconstituted Silk Fiber from Aqueous Silk Fibroin Solution.” *Materials Science and Engineering: C* 29 (7): 2270–74. https://doi.org/10.1016/j.msec.2009.05.012.

Cestari, Marília, Vinícius Muller, Jean Henrique da Silva Rodrigues, Celso V. Nakamura, Adley F. Rubira, and Edvani C. Muniz. 2014. “Preparing Silk Fibroin Nanofibers through Electrospinning: Further Heparin Immobilization toward Hemocompatibility Improvement.” *Biomacromolecules* 15 (5): 1762–67. https://doi.org/10.1021/bm500132g.

Cho, Se Youn, Min Eui Lee, Youngeun Choi, and Hyoung-Joon Jin. 2014. “Cellulose Nanofiber-Reinforced Silk Fibroin Composite Film with High Transparency.” *Fibers and Polymers* 15 (2): 215–19. https://doi.org/10.1007/s12221-014-0215-y.

Chouhan, Dimple, Bijayshree Chakraborty, Samit K. Nandi, and Biman B. Mandal. 2017. “Role of Non-Mulberry Silk Fibroin in Deposition and Regulation of Extracellular Matrix towards Accelerated Wound Healing.” *Acta Biomaterialia* 48: 157–74. https://doi.org/10.1016/j.actbio.2016.10.019.

De Santis, Felice, and Roberto Pantani. 2013. “Optical Properties of Polypropylene upon Recycling.” *The Scientific World Journal* 2013 (October). https://doi.org/10.1155/2013/354093.

Doutch, James, Andrew J. Quantock, Valerie A. Smith, and Keith M. Meek. 2008. “Light Transmission in the Human Cornea as a Function of Position across the Ocular Surface: Theoretical and Experimental Aspects.” *Biophysical Journal* 95 (11): 5092–99. https://doi.org/10.1529/biophysj.108.132316.

Echave, Mari C., Laura Saenz del Burgo, Jose L. Pedraz, and Gorka Orive. 2017. “Gelatin as Biomaterial for Tissue Engineering.” *Current Pharmaceutical Design* 23 (24): 3567–84. https://doi.org/10.2174/0929867324666170511123101.

Edwards, Aurélie, and Mark R. Prausnitz. 1998. “Fiber Matrix Model of Sclera and Corneal Stroma for Drug Delivery to the Eye.” *AIChE Journal* 44 (1): 214–25. https://doi.org/10.1002/aic.690440123.

Fan, Linpeng, Hongsheng Wang, Kuihua Zhang, Chuanglong He, Zengxiao Cai, and Xiumei Mo. 2012. “Regenerated Silk Fibroin Nanofibrous Matrices Treated with 75% Ethanol Vapor for Tissue-Engineering Applications.” *Journal of Biomaterials Science. Polymer Edition* 23 (1–4): 497–508. https://doi.org/10.1163/092050610X552771.

Farasatkia, Asal, Mahshid Kharaziha, Fakhreddin Ashrafizadeh, and Sahar Salehi. 2021. “Transparent Silk/Gelatin Methacrylate (GelMA) Fibrillar Film for Corneal Regeneration.” *Materials Science and Engineering: C* 120 (January): 111744. https://doi.org/10.1016/j.msec.2020.111744.

Freddi, Giuliano, Maria Romanò, Maria Rosaria Massafra, and Masuhiro Tsukada. 1995. “Silk Fibroin/Cellulose Blend Films: Preparation, Structure, and Physical Properties.” *Journal of Applied Polymer Science* 56 (12): 1537–45. https://doi.org/10.1002/app.1995.070561203.

Freegard, Timothy J. 1997. “The Physical Basis of Transparency of the Normal Cornea.” *Eye* 11 (4): 465–71. https://doi.org/10.1038/eye.1997.127.

Gandhi, Milind, Heejae Yang, Lauren Shor, and Frank Ko. 2009. “Post-Spinning Modification of Electrospun Nanofiber Nanocomposite from Bombyx Mori Silk and Carbon Nanotubes.” *Polymer* 50 (8): 1918–24. https://doi.org/10.1016/j.polymer.2009.02.022.

Gui-Bo, Yin, Zhang You-Zhu, Wang Shu-Dong, Shi De-Bing, Dong Zhi-Hui, and Fu Wei-Guo. 2009. "Study of the Electrospun PLA/Silk Fibroin-Gelatin Composite Nanofibrous Scaffold for Tissue Engineering." *Journal of Biomedical Materials Research Part A* 9999A: NA-NA. https://doi.org/10.1002/jbm.a.32496.

Haider, Adnan, Sajjad Haider, and Inn-Kyu Kang. 2018. "A Comprehensive Review Summarizing the Effect of Electrospinning Parameters and Potential Applications of Nanofibers in Biomedical and Biotechnology." *Arabian Journal of Chemistry* 11 (8): 1165–88. https://doi.org/10.1016/j.arabjc.2015.11.015.

Hashimoto, Yoshihide, Seiichi Funamoto, Shuji Sasaki, Takako Honda, Shinya Hattori, Kwangwoo Nam, Tsuyoshi Kimura, et al. 2010. "Preparation and Characterization of Decellularized Cornea Using High-Hydrostatic Pressurization for Corneal Tissue Engineering." *Biomaterials* 31 (14): 3941–48. https://doi.org/10.1016/j.biomaterials.2010.01.122.

Hazra, Sarbani, Sudip Nandi, Deboki Naskar, Rajdeep Guha, Sushovan Chowdhury, Nirparaj Pradhan, Subhas C. Kundu, and Aditya Konar. 2016. "Non-Mulberry Silk Fibroin Biomaterial for Corneal Regeneration." *Scientific Reports* 6 (1): 21840. https://doi.org/10.1038/srep21840.

Hu, Xiao, David Kaplan, and Peggy Cebe. 2006. "Determining Beta-Sheet Crystallinity in Fibrous Proteins by Thermal Analysis and Infrared Spectroscopy." *Macromolecules* 39 (18): 6161–70. https://doi.org/10.1021/ma0610109.

Ibrahim, Dina M., Andreas Kakarougkas, and Nageh K. Allam. 2017. "Recent Advances on Electrospun Scaffolds as Matrices for Tissue-Engineered Heart Valves." *Materials Today Chemistry* 5 (September): 11–23.

https://doi.org/10.1016/j.mtchem.2017.05.001.

Ifuku, Shinsuke, Akiko Ikuta, Mayumi Egusa, Hironori Kaminaka, Hironori Izawa, Minoru Morimoto, and Hiroyuki Saimoto. 2013. “Preparation of High-Strength Transparent Chitosan Film Reinforced with Surface-Deacetylated Chitin Nanofibers.” *Carbohydrate Polymers* 98 (1): 1198–1202. https://doi.org/10.1016/j.carbpol.2013.07.033.

Jin, H.-J., J. Park, V. Karageorgiou, U.-J. Kim, R. Valluzzi, P. Cebe, and D. L. Kaplan. 2005. “Water-Stable Silk Films with Reduced β-Sheet Content.” *Advanced Functional Materials* 15 (8): 1241–47. https://doi.org/10.1002/adfm.200400405.

Kishimoto, Yuki, Takanori Kobashi, Shigeru Yamanaka, Hideaki Morikawa, and Yasushi Tamada. 2018. “Comparisons between Silk Fibroin Nonwoven Electrospun Fabrics Using Aqueous and Formic Acid Solutions.” *International Journal of Polymeric Materials and Polymeric Biomaterials* 67 (7): 462–67. https://doi.org/10.1080/00914037.2017.1342253.

Kishimoto, Yuki, Hideaki Morikawa, Shigeru Yamanaka, and Yasushi Tamada. 2017. “Electrospinning of Silk Fibroin from All Aqueous Solution at Low Concentration.” *Materials Science and Engineering: C* 73 (April): 498–506. https://doi.org/10.1016/j.msec.2016.12.113.

Koeppel, Andreas, Peter R. Laity, and Chris Holland. 2018. “Extensional Flow Behaviour and Spinnability of Native Silk.” *Soft Matter* 14 (43): 8838–45. https://doi.org/10.1039/C8SM01199K.

Komai, Y., and T. Ushiki. 1991. “The Three-Dimensional Organization of Collagen Fibrils in the Human Cornea and Sclera.” *Investigative Ophthalmology & Visual Science* 32 (8): 2244–58.

Kong, Bin, and Shengli Mi. 2016. “Electrospun Scaffolds for Corneal Tissue Engineering: A Review.” *Materials* 9 (8): 614. https://doi.org/10.3390/ma9080614.

Kong, Bin, Wei Sun, Guoshi Chen, Song Tang, Ming Li, Zengwu Shao, and Shengli Mi. 2017. “Tissue-Engineered Cornea Constructed with Compressed Collagen and Laser-Perforated Electrospun Mat.” *Scientific Reports* 7 (1): 970. https://doi.org/10.1038/s41598-017-01072-0.

Lerman, S. 1984. “Biophysical Aspects of Corneal and Lenticular Transparency.” *Current Eye Research* 3 (1): 3–14. https://doi.org/10.3109/02713688408997182.

Li, D., and Y. Xia. 2004. “Electrospinning of Nanofibers: Reinventing the Wheel?” *Advanced Materials* 16 (14): 1151–70. https://doi.org/10.1002/adma.200400719.

Lynch, Amy P., Samantha L. Wilson, and Mark Ahearne. 2016. “Dextran Preserves Native Corneal Structure During Decellularization.” *Tissue Engineering. Part C, Methods* 22 (6): 561–72. https://doi.org/10.1089/ten.TEC.2016.0017.

Matthyssen, Steffi, Bert Van den Bogerd, Sorcha Ní Dhubhghaill, Carina Koppen, and Nadia Zakaria. 2018. “Corneal Regeneration: A Review of Stromal Replacements.” *Acta Biomaterialia* 69 (March): 31–41. https://doi.org/10.1016/j.actbio.2018.01.023.

Meek, Keith M. 2009. “Corneal Collagen—Its Role in Maintaining Corneal Shape and Transparency.” *Biophysical Reviews* 1 (2): 83–93. https://doi.org/10.1007/s12551-009-0011-x.

Michalak, Monika, Leszek Łatka, Patrycja Szymczyk, and Paweł Sokołowski. 2017. "Computational Image Analysis of Suspension Plasma Sprayed YSZ Coatings." *ITM Web of Conferences* 15: 06004. https://doi.org/10.1051/itmconf/20171506004.

Min, Byung-Moo, Lim Jeong, Kuen Yong Lee, and Won Ho Park. 2006. "Regenerated Silk Fibroin Nanofibers: Water Vapor-Induced Structural Changes and Their Effects on the Behavior of Normal Human Cells." *Macromolecular Bioscience* 6 (4): 285–92. https://doi.org/10.1002/mabi.200500246.

Min, Byung-Moo, Gene Lee, So Hyun Kim, Young Sik Nam, Taek Seung Lee, and Won Ho Park. 2004. "Electrospinning of Silk Fibroin Nanofibers and Its Effect on the Adhesion and Spreading of Normal Human Keratinocytes and Fibroblasts in Vitro." *Biomaterials* 25 (7–8): 1289–97. https://doi.org/10.1016/j.biomaterials.2003.08.045.

Minoura, Norihiko, Masuhiro Tsukada, and Masanobu Nagura. 1990. "Physico-Chemical Properties of Silk Fibroin Membrane as a Biomaterial." *Biomaterials* 11 (6): 430–34. https://doi.org/10.1016/0142-9612(90)90100-5.

Mitropoulos, Alexander N., Benedetto Marelli, Chiara E. Ghezzi, Matthew B. Applegate, Benjamin P. Partlow, David L. Kaplan, and Fiorenzo G. Omenetto. 2015. "Transparent, Nanostructured Silk Fibroin Hydrogels with Tunable Mechanical Properties." *ACS Biomaterials Science & Engineering* 1 (10): 964–70. https://doi.org/10.1021/acsbiomaterials.5b00215.

Mohammadzadehmoghadam, Soheila, and Yu Dong. 2019. "Fabrication and Characterization of Electrospun Silk Fibroin/Gelatin Scaffolds Crosslinked With Glutaraldehyde Vapor." *Frontiers in Materials* 6. https://doi.org/10.3389/fmats.2019.00091.

Murphy, Ciara M., Matthew G. Haugh, and Fergal J. O'Brien. 2010. "The Effect of Mean Pore Size on Cell Attachment, Proliferation and Migration in Collagen-Glycosaminoglycan Scaffolds for Bone Tissue Engineering." *Biomaterials* 31 (3): 461–66. https://doi.org/10.1016/j.biomaterials.2009.09.063.

Nogi, Masaya, Shinichiro Iwamoto, Antonio Norio Nakagaito, and Hiroyuki Yano. 2009. "Optically Transparent Nanofiber Paper." *Advanced Materials* 21 (16): 1595–98. https://doi.org/10.1002/adma.200803174.

Okhawilai, Manunya, Ratthapol Rangkupan, Sorada Kanokpanont, and Siriporn Damrongsakkul. 2010. "Preparation of Thai Silk Fibroin/Gelatin Electrospun Fiber Mats for Controlled Release Applications." *International Journal of Biological Macromolecules* 46 (5): 544–50. https://doi.org/10.1016/j.ijbiomac.2010.02.008.

Qazi, Yureeda, Gilbert Wong, Bryan Monson, Jack Stringham, and Balamurali K. Ambati. 2010. "Corneal Transparency: Genesis, Maintenance and Dysfunction." *Brain Research Bulletin* 81 (2–3): 198–210. https://doi.org/10.1016/j.brainresbull.2009.05.019.

Qi, Yu, Hui Wang, Kai Wei, Ya Yang, Ru-Yue Zheng, Ick Kim, and Ke-Qin Zhang. 2017. "A Review of Structure Construction of Silk Fibroin Biomaterials from Single Structures to Multi-Level Structures." *International Journal of Molecular Sciences* 18 (3): 237. https://doi.org/10.3390/ijms18030237.

Rockwood, Danielle N., Rucsanda C. Preda, Tuna Yücel, Xiaoqin Wang, Michael L. Lovett, and David L. Kaplan. 2011. "Materials Fabrication from Bombyx Mori Silk Fibroin." *Nature Protocols* 6 (10). https://doi.org/10.1038/nprot.2011.379.

Rose, James B., Settimio Pacelli, Alicia J. El Haj, Harminder S. Dua, Andrew Hopkinson, Lisa J. White, and Felicity R. A. J. Rose. 2014. “Gelatin-Based Materials in Ocular Tissue Engineering.” *Materials* 7 (4): 3106–35. https://doi.org/10.3390/ma7043106.

Sahi, Ajay Kumar, Neelima Varshney, Suruchi Poddar, and Sanjeev Kumar Mahto. 2020. “Comparative Behaviour of Electrospun Nanofibers Fabricated from Acid and Alkaline Hydrolysed Gelatin: Towards Corneal Tissue Engineering.” *Journal of Polymer Research* 27 (11): 344. https://doi.org/10.1007/s10965-020-02307-x.

Shan, Ying-Hui, Li-Hua Peng, Xin Liu, Xi Chen, Jie Xiong, and Jian-Qing Gao. 2015. “Silk Fibroin/Gelatin Electrospun Nanofibrous Dressing Functionalized with Astragaloside IV Induces Healing and Anti-Scar Effects on Burn Wound.” *International Journal of Pharmaceutics* 479 (2): 291–301. https://doi.org/10.1016/j.ijpharm.2014.12.067.

Shen, Gaotian, Xingyou Hu, Guoping Guan, and Lu Wang. 2015. “Surface Modification and Characterisation of Silk Fibroin Fabric Produced by the Layer-by-Layer Self-Assembly of Multilayer Alginate/Regenerated Silk Fibroin.” *PLOS ONE* 10 (4): e0124811. https://doi.org/10.1371/journal.pone.0124811.

Sun, Mingyue, Xiaoting Sun, Ziyuan Wang, Shuyu Guo, Guangjiao Yu, and Huazhe Yang. 2018. “Synthesis and Properties of Gelatin Methacryloyl (GelMA) Hydrogels and Their Recent Applications in Load-Bearing Tissue.” *Polymers* 10 (11). https://doi.org/10.3390/polym10111290.

Taddei, Paola, Valeria Chiono, Anna Anghileri, Giovanni Vozzi, Giuliano Freddi, and Gianluca Ciardelli. 2013. “Silk Fibroin/Gelatin Blend Films Crosslinked with Enzymes for Biomedical Applications.” *Macromolecular Bioscience* 13 (11): 1492–1510. https://doi.org/10.1002/mabi.201300156.

Tonsomboon, Khaow, and Michelle L. Oyen. 2013. “Composite Electrospun Gelatin Fiber-Alginate Gel Scaffolds for Mechanically Robust Tissue Engineered Cornea.” *Journal of the Mechanical Behavior of Biomedical Materials* 21 (May): 185–94. https://doi.org/10.1016/j.jmbbm.2013.03.001.

Varshney, Neelima, Ajay Kumar Sahi, Suruchi Poddar, and Sanjeev Kumar Mahto. 2020. “Soy Protein Isolate Supplemented Silk Fibroin Nanofibers for Skin Tissue Regeneration: Fabrication and Characterization.” *International Journal of Biological Macromolecules* 160 (October): 112–27. https://doi.org/10.1016/j.ijbiomac.2020.05.090.

Varshney, Neelima, Ajay Kumar Sahi, Kiran Yellappa Vajanthri, Suruchi Poddar, Chelladurai Karthikeyan Balavigneswaran, Arumugam Prabhakar, Vivek Rao, and Sanjeev Kumar Mahto. 2019. “Culturing Melanocytes and Fibroblasts within Three-Dimensional Macroporous PDMS Scaffolds: Towards Skin Dressing Material.” *Cytotechnology* 71 (1): 287–303. https://doi.org/10.1007/s10616-018-0285-6.

Wang, Mao, Hyoung-Joon Jin, David L. Kaplan, and Gregory C. Rutledge. 2004. “Mechanical Properties of Electrospun Silk Fibers.” *Macromolecules* 37 (18): 6856–64. https://doi.org/10.1021/ma048988v.

Yang, Mingying, Yajun Shuai, Wen He, Sijia Min, and Liangjun Zhu. 2012. “Preparation of Porous Scaffolds from Silk Fibroin Extracted from the Silk Gland of Bombyx Mori (B. Mori).” *International Journal of Molecular Sciences* 13 (6): 7762–75. https://doi.org/10.3390/ijms13067762.

Yao, Li, Thomas W. Haas, Anthony Guiseppi-Elie, Gary L. Bowlin, David. G. Simpson, and Gary E. Wnek. 2003. “Electrospinning and Stabilization of Fully Hydrolyzed

Poly(Vinyl Alcohol) Fibers." *Chemistry of Materials* 15 (9): 1860–64. https://doi.org/10.1021/cm0210795.

Ye, Juan, Xin Shi, Xiaoyi Chen, Jiajun Xie, Changjun Wang, Ke Yao, Changyou Gao, and Zhongru Gou. 2014. "Chitosan-Modified, Collagen-Based Biomimetic Nanofibrous Membranes as Selective Cell Adhering Wound Dressings in the Treatment of Chemically Burned Corneas." *Journal of Materials Chemistry B* 2 (27): 4226–36. https://doi.org/10.1039/C3TB21845G.

Yin-Guibo, Zhang-Youzhu, Bao-Weiwei, Wu-Jialin, Shi De-bing, Dong Zhi-hui, and Fu Wei-guo. 2009. "Study on the Properties of the Electrospun Silk Fibroin/Gelatin Blend Nanofibers for Scaffolds." *Journal of Applied Polymer Science* 111 (3): 1471–77. https://doi.org/10.1002/app.28963.

Yusoff, Noor Izyan Syazana Mohd, Mat Uzir Wahit, Juhana Jaafar, and Tuck Whye Wong. 2019. "Structural and Characterization Studies of Insoluble Thai Bombyx Mori Silk Fibroin Films." https://doi.org/10.11113/MJFAS.V15N2019.1223.

Zeng, Y., J. Yang, K. Huang, Z. Lee, and X. Lee. 2001. "A Comparison of Biomechanical Properties between Human and Porcine Cornea." *Journal of Biomechanics* 34 (4): 533–37. https://doi.org/10.1016/s0021-9290(00)00219-0.

Zhao, Guoxu, Xiaohui Zhang, Tian Jian Lu, and Feng Xu. 2015. "Recent Advances in Electrospun Nanofibrous Scaffolds for Cardiac Tissue Engineering." *Advanced Functional Materials* 25 (36): 5726–38. https://doi.org/10.1002/adfm.201502142.